Title page

Title

naRNA is a canonical neutrophil extracellular trap (NET) component and novel inflammation-amplifying composite DAMP

Running title

naRNA – canonical NET component and composite DAMP

Authors

Francesca Bork[1], Carsten L. Greve[1], Christine Youn[2], Sirui Chen[1], Yu Wang[2], Masoud Nasri[3], Jule Focken[4], Jasmin Scheurer[4], Pujan Engels[1], Marissa Dubbelaar[1,5], Katharina Hipp[6], Birgit Schittek[4,7,8], Stefanie Bugl[1], Markus W. Löffler[1,7,9], Julia Skokowa[3,7], Nathan K. Archer[2] (ORCID: 0000-0002-8212-8985), Alexander N.R. Weber[1,7,8]* (ORCID: 0000-0002-8627-7056)

Author information

[1]Interfaculty Institute for Cell Biology, Department of Immunology, University of Tübingen, Auf der Morgenstelle 15, 72076 Tübingen, Germany

[2]Department of Dermatology, Johns Hopkins University School of Medicine, Baltimore, MD 21231, USA

[3]Division of Translational Oncology, Department of Oncology, Hematology, Clinical Immunology and Rheumatology, University Hospital Tübingen, Otfried-Müller Str. 10, 72076 Tübingen, Germany

[4]Division of Dermatooncology, Department of Dermatology, University Hospital Tübingen, Liebermeisterstr. 25, 72076 Tübingen, Germany

[5]Quantitative Biology Center (QBiC), University of Tübingen, Auf der Morgenstelle 10, 72076 Tübingen, Germany

[6]Electron Microscopy Facility, Max Planck Institute for Biology Tübingen, Max-Planck-Ring 5, 72076 Tübingen, Germany

[7]iFIT – Cluster of Excellence (EXC 2180) "Image-Guided and Functionally Instructed Tumor Therapies", University of Tübingen, Germany

29 [8]CMFI – Cluster of Excellence (EXC 2124) "Controlling microbes to fight infection", University of
30 Tübingen, Germany.

31 [9]Department of General, Visceral and Transplant Surgery, University Hospital Tübingen, Hoppe-
32 Seyler-Str. 3, 72076 Tübingen, Germany and Department of Clinical Pharmacology, University
33 Hospital Tübingen, Auf der Morgenstelle 8, 72076 Tübingen, Germany

34

35 **Corresponding Author**

36 Alexander N. R. Weber, Interfaculty Institute for Cell Biology, Department of Immunology, University
37 of Tübingen, Auf der Morgenstelle 15, 72076 Tübingen, Germany. Tel.: +49 7071 29 87623. Fax: +49
38 7071 29 4579. Email: alexander.weber@uni-tuebingen.de; ORCID: 0000-0002-8627-7056, Twitter
39 @aweberlab

Abstract

Neutrophil extracellular traps (NETs) have emerged as a key feature of cellular innate immunity mediated by polymorphonuclear neutrophils (PMNs), the primary leukocyte population in humans. Forming web-like structures composed of DNA, histones, and antimicrobial proteins, NETs trap and kill microbial invaders and thus enhance host defense. However, they have also been linked to inflammatory states, e.g., in atherosclerosis or psoriasis. Whilst DNA has been in focus as a primary structural component of NETs, we here characterize naRNA (NET-associated RNA), as a new canonical, abundant, and largely unexplored NET component. naRNA decorated all types of NETs in complex with the antimicrobial peptide LL37. In fact, naRNA was pre-associated with LL37 intracellularly as a 'composite' danger-associated molecular pattern (DAMP) prior to neutrophil activation. Externalized, naRNA propagated NET formation in naïve PMN, dependent on TLR8 in humans and Tlr13 in mice, in vitro and in vivo. TLR8/Tlr13 signaling contributed significantly to the highly sensitive pro-inflammatory response to naRNA, involving tissue cells, like keratinocytes, and other immune cell types, such as macrophages. Those responses could be blocked by inhibition and genetic ablation of RNA receptors or RNase treatment. Importantly, in vivo naRNA strongly drove skin inflammation whereas genetic ablation of RNA sensing drastically ameliorated skin inflammation in the imiquimod psoriasis model. Our data highlight naRNA as a novel composite DAMP signaling and amplifying neutrophil activation. Moreover, naRNA emerges as the likely driver of inflammation in conditions previously linked to NETs and extracellular RNA, suggesting blockade of TLR-mediated RNA sensing as potential new intervention target.

Graphical abstract

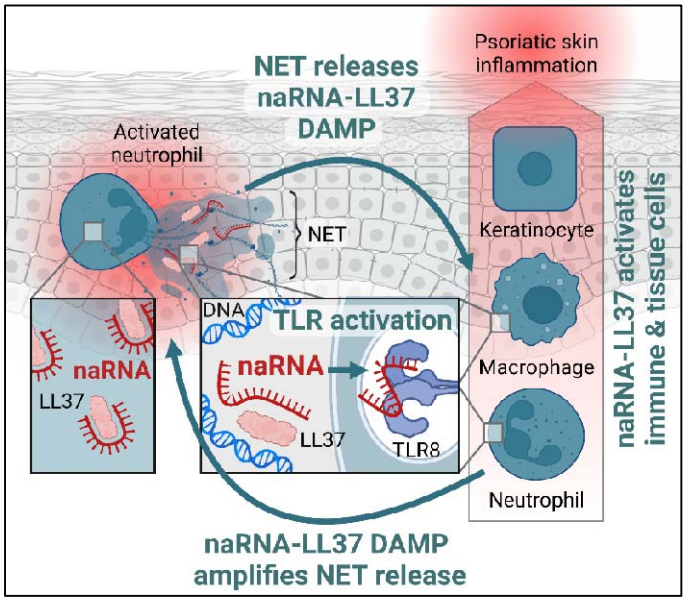

Created with biorender.com

63 **Introduction**

64 The formation of Neutrophil Extracellular Traps (NETs), since its discovery in 2004 [1], has emerged as a
65 fascinating phenomenon of host defense. Hereby neutrophils, the primary leukocyte population,
66 extrude their genomic DNA to form web-like structures that, similar to barbed wire roadblocks, trap
67 and kill microbial invaders such as bacteria or fungi [2]. DNA is thus a defining structural and functional
68 feature of NETs. Additionally, DNA-associated proteins, histones and HMGB-1, antimicrobial peptides
69 like LL37 and enzymes such as myeloperoxidase (MPO) are released during the formation of NETs
70 and contribute to their antimicrobial function [2]. More than 1,000 publications on NETs have sought
71 to detail the multi-faceted phenomenon and the processes that lead to its execution [3]. However,
72 with the main focus devoted to DNA and protein components, another primary cellular biomolecule,
73 RNA, has so far received very little attention in vertebrates. Interestingly, a study in insects showed
74 that hemocytes (macrophage-like immune cells) can release both DNA and RNA in NET-like
75 structures during microbe-triggered clotting reactions, and in response to extracellular RNA or DNA [4].
76 Our lab recently provided evidence of a responsiveness of human polymorphonuclear neutrophils
77 (PMNs) to RNA, but not DNA, in combination with the antimicrobial peptide LL37, fueling neutrophil
78 activation [5]. In addition, earlier work described a role for DNA- and RNA-LL37 complexes in the
79 activation of plasmacytoid dendritic cells [6, 7]. This has given rise to the notion that under certain
80 conditions tolerance to self-DNA and RNA can be broken[8], involving the nucleic acid-sensing TLR7,
81 TLR8 (ssRNA) and TLR9 (DNA) in humans, and Tlr7, Tlr13 and Tlr9 in mice [9, 10]. In general, many roles
82 have been ascribed to so-called extracellular RNA (exRNA), for example, macrophage polarization,
83 recruitment of leukocytes to the site of inflammation, leukocyte rolling at the vascular endothelium,
84 as well as integrin-mediated firm adhesion of immune cells and promotion of thrombosis [11].
85 Additionally, exRNA is considered as a reliable biomarker for various diseases such as cancer or
86 cardiovascular pathologies [12, 13]. However, RNA being considered a short-lived biomolecule,
87 physiological sources of exRNA have been somewhat unclear. Under sterile conditions, vascular
88 injury, tissue damage, or ischemia have been suggested to trigger release of exRNA along with other
89 cellular material [11]it remains unclear it remains unclear whether these relatively slow processes could
90 amount to physiologically detectable exRNA amounts in the serum of patients, or whether a rapid,
91 as-yet unidentified process of RNA extrusion would have to be postulated.

92 We speculated that RNA contained in NETs, so-called NET-associated RNA or naRNA, might lead to a
93 feed-forward loop of rapidly expanding NET release amongst neutrophils which might also engulf
94 additional tissue or immune cells able to respond to exRNA. We show here that naRNA drives such a
95 self-amplifying loop not only engaging PMNs but also macrophages, and keratinocytes. naRNA
96 responsiveness was dependent on *TLR8* and *Tlr13* in human and murine myeloid immune cells,

97 respectively. Interestingly, naRNA appears pre-complexed to LL37 as a novel composite DAMP.
98 Notably, in mice naRNA caused considerable skin inflammation in a Tlr13-dependent manner.
99 Additionally, in a well-established model of psoriatic skin inflammation, genetic ablation of RNA
100 sensing strongly ameliorated skin inflammation, highlighting naRNA as a potent damage associate
101 molecular pattern (DAMP) amplifying PMN activation and alerting tissue and other immune cells.

102 Results

103 naRNA is a common component of NETs

104 To first investigate whether naRNA was a common component of NETs, we compared NETs from
105 human PMNs formed in response to the well-defined molecular agonists PMA, different complexes
106 of LL37 with purified RNA (synthetic, as well as total fungal and bacterial RNA from *S. aureus* and *C.*
107 *albicans*, respectively), nigericin and the live pathogen *C. albicans*. Confocal microscopy analysis
108 using the well-characterized rRNA-specific antibody, Y10b [14], revealed the presence of RNA in all
109 corresponding NETs, independent of stimulus and whether NET formation was 'suicidal' or not [3] (Fig.
110 1A, quantified in B; control in Fig. S1A): the RNA signal was readily detectable along the web-like DNA
111 threads in human NETs. Similar results were obtained in NETs released by murine bone marrow-
112 derived PMNs (BM-PMNs, Fig. 1C; control Fig. S1B). To avoid the use of staining reagents, we also
113 metabolically labeled primary human hematopoietic stem cells (HSCs) with 5-ethynyluridine (5-EU), a
114 nucleotide that can be incorporated in cellular RNA but not DNA, and that is amenable to labeling by
115 click chemistry [15]. These HSCs were then differentiated to neutrophils [16] and the differentiation
116 validated by microscopy and flow cytometric analysis (Fig. S1C, D). NETs released from HSC-derived
117 PMNs could indeed be labeled with click reagents conferring a fluorescent label only when grown in
118 5-EU-containing medium (Fig. 1D). Moreover, the overlap between click-label and rRNA confirmed
119 the specificity of the staining with anti-rRNA antibodies and indicated that naRNA contained rRNA
120 but also other types of cellular RNAs. This experiment also unequivocally confirmed that upon PMN
121 stimulation, cellular RNA is turned into a component of the NET, wherein it decorates the fine, web-
122 like DNA structures. The localization of naRNA on DNA strands was further confirmed by high-
123 resolution fluorescence microscopy and 3D analysis (AiryScan, Fig. 1E and Supplemental Movie S1) as
124 well as scanning electron microscopy (SEM, Fig. 1F; controls Fig. S1E). Extraction of naRNA from PMA-
125 induced NETs (Fig. 1G) and subsequent RNA-sequencing analysis confirmed that purified naRNA
126 contained multiple RNA types, with noticeably more non-ribosomal RNA than the corresponding
127 total cellular RNA of PMNs (Fig. 1H). Collectively, these results indicate that naRNA is a canonical
128 component of NETs released upon multiple stimuli from both human and murine neutrophils.

129 naRNA is a potent 'composite' DAMP propagating NET formation in primary PMNs

130 A primary function of NETs is host defense by trapping and killing bacteria. Therefore, we first
131 explored if naRNA participated in this process [1]. However, the antibacterial effect of NETs on live
132 *Staphylococcus aureus* (evidenced by lower CFUs compared to resting PMNs) was similar to that of
133 RNase-treated NETs, whereas DNase digestion reduced the drop in CFU discernibly but non-
134 significantly (Fig. S2A). Consequently, we turned our attention to a possible role of naRNA as a
135 DAMP, since primary PMNs can respond to synthetic RNA-LL37 complexes with NET formation, and
136 our earlier analysis indicated that NETs also contain LL37 [5]. To prepare a naRNA-containing stimulant,
137 PMA-induced NETs were prepared as described in Methods and the original stimulus, PMA, removed
138 by extensive washing before harvesting. Interestingly, these 'PMA NETs', when applied to naïve
139 PMNs from another donor, potently induced new NETs (Fig. 2B, quantified in C, controls in Fig. S2B).
140 Treatment with an RNase inhibitor enhanced the stimulatory effect of PMA NETs rendering a 1:500
141 dilution of PMA-NETs more effective than a 1:50 dilution of non-treated PMA-NETs (Fig. 2B, C,
142 controls Fig. S2B). Interestingly, similar NET preparations from mock-treated PMNs (here referred to
143 as 'mock NETs') did not stimulate NET formation under the same experimental conditions. To rule
144 out the possibility that residual PMA in PMA NETs could be responsible for the observed stimulatory
145 effects, RNase treatment was also performed which strongly reduced NET formation (Fig. 2D,
146 quantified in E; controls Fig. S2C).. The destruction of naRNA in NETs was further confirmed by rapid
147 loss of the RNA signal (using the RNA-selective dye, SYTO RNAselect [5] in time-lapse digestion analysis
148 (Supplemental Movie S2). Bearing in mind that PMNs do not respond to DNA or DNA-LL37 complexes
149 [5], the opposing effects of RNase inhibitor and RNase treatments thus clearly indicated naRNA (and
150 not DNA) to be the relevant immunostimulatory component for NETs to drive the activation of naïve
151 PMNs. In line with our previous work showing that synthetic RNA or LL37 alone cannot trigger PMN
152 activation [5], purified 'naked' naRNA isolated from PMA NETs (*cf.* Fig. 1G) was unable to activate NET
153 formation; however, re-complexing with exogenous LL37 was sufficient to restore NET formation
154 (Fig. 2F, controls in Fig. S2D). We next investigated whether in NETs, naRNA co-localized with LL37.
155 Strong co-localization was evident in confocal microscopy analysis (Fig. 2G) and confirmed by
156 Pearson's colocalization analysis (Fig. 2H). Additional line plot analysis of PMA-stimulated PMN
157 revealed that RNA and LL37 did in fact co-localize in NETs, i.e., after extrusion (Fig. S2E). Surprisingly,
158 in unstimulated PMNs naRNA and LL37 showed even greater colocalization (Fig. 2H) and shared co-
159 localization maxima, suggesting pre-association before extrusion (Fig. 2I, Fig. S2E). rRNA and LL37
160 double staining on ultrathin (50-60 nm) sections of resting PMN confirmed the reported localization
161 of LL37 to neutrophil granules [17], but also the unexpected concomitant presence of naRNA in the
162 same structures (Fig. 2J). Transmission electron microscopy combined with double staining of rRNA
163 Y10b and LL37 using two different immunogold sizes corroborated this further at even higher
164 magnification (Fig. 2K, Fig. S2F). The concept of pre-packaging of RNA with LL37 in specific

165 compartments also fits with the RNAseq data showing that certain RNA types are lost upon release
166 (*cf.* Fig. 1H), probably because they are not bound to LL37. Collectively, naRNA appears to be LL37-
167 pre-associated, and hence a 'composite' DAMP, enabling PMN activation and NET propagation.

168 **naRNA DAMP activity is dependent on RNA sensors TLR8/Tlr13**

169 To validate naRNA as an immunostimulatory RNA component from the receptor side, we turned to
170 HEK293T cells which do not respond to RNA, unless transfected with plasmids encoding the human
171 ssRNA sensors TLR7 or TLR8 [18]. NF-κB reporter assays revealed that TLR7 or TLR8- (both ssRNA
172 sensors) but not TLR9 (human DNA sensor)-transfected HEK293T cells stimulated with PMA NETs or
173 mock NETs showed robust NF-κB activity only for PMA NETs (Fig. 3A). R848 (TLR7 and TLR8 agonist)
174 and TL8 or ssRNA+DOTAP (both TLR8 agonists) served as controls. Of note, compared to its cognate
175 agonist, CpG, the DNA sensor TLR9 was only poorly activated by PMA NETs, indicating that naRNA is a
176 superior immune stimulant compared to NET DNA in this system. Indeed, the observed NET response
177 of primary PMNs (Fig. 3B, quantified in C, and Fig. S3A) could be completely blocked by the TLR8-
178 specific inhibitor, CU-CPT9a [19], similar to the effects of the non-specific inhibitor, Cl-amidine, a PAD4
179 inhibitor which also blocked the response to PMA (Fig. 3C and S3A). This revealed the RNA sensor
180 TLR8 [20] to be the specific naRNA receptor in primary human PMNs. We further genetically validated
181 the involvement of RNA sensing in naRNA-mediated NET propagation using BM-PMNs from *Unc93b1*-
182 or *Tlr13*-defective mice: whereas in *Unc93b1*-defective mice signaling of all endosomal TLRs is
183 abrogated [21], mice lacking *Tlr13,* the murine equivalent of TLR8 [9], specifically lack ssRNA sensing [22].
184 Confocal microscopy analysis showed that WT BM-PMNs responded readily to both PMA (used as
185 control) and PMA NETs, whereas *Unc93b1* (Fig. S3B) or *Tlr13* KO PMNs (Fig. 3D, quantified in E) only
186 responded to the TLR-independent PMA control but not PMA NETs. Additionally, naïve BM-PMNs
187 from *Tlr9* KO mice, which lack DNA sensing, responded to both PMA and PMA NETs with NET
188 formation just like WT BM-PMNs (Fig. S3C), emphasizing the redundancy of DNA vs the key role of
189 naRNA in the self-propagating properties of NETs. This receptor analysis unequivocally confirmed
190 naRNA to be a primary immune stimulant in NETs.

191 **PMN-derived naRNA triggers broader immune cell and keratinocyte activation**

192 Given the potent effect of naRNA on naïve PMNs (*cf.* Fig. 3B-E) and the ability of human
193 macrophages to sense RNA via TLR8 [23], we hypothesized that naRNA might also directly activate
194 macrophages, which are rapidly recruited at the sites of PMN activation in peripheral tissues [24],
195 contributing to an inflammatory process in vivo. We thus assessed the effects of naRNA on
196 genetically modified macrophage-like cell lines: BlaER1 macrophages [25] responded to PMA NETs but
197 not mock NETs with IL-8 release, and this was TLR8-dependent as evidenced by comparisons of WT
198 and *TLR8*-edited BlaER1 cells (Fig. 3F). Use of a naRNA-stabilizing RNase inhibitor during NET

199 preparation (*cf.* Fig. 2B) drastically increased the potency of PMA NETs on these macrophages.
200 Additionally, TLR8 and TLR7-edited THP-1 macrophage-like cells [26] responded to PMA NETs with
201 lower relative IL-8 release than WT THP-1 cells (Fig. S4A), confirming RNA as the active agent in
202 monocyte/macrophage activation. Human peripheral blood mononuclear cells (PBMCs) were also
203 stimulated with different NET preparations. RNA-stabilized PMA NETs consistently elicited higher
204 TNF, IL-6 and IL-8 levels than non-stabilized PMA- or mock NETs (Fig. S4B-D). However, this effect was
205 not sensitive to the TLR8 inhibitor Cu-CPT9a, which is consistent with the ability of TLR7 to also sense
206 naRNA (*cf.* Fig. 3A) and possibly due to a mixture of cells being present. Further analysis revealed that
207 the natural killer (NK) cell line NK-92 MI showed low IFNγ release in response to RNA-stabilized PMA
208 NETs (Fig. S4E). Collectively, our results show that the RNA component of NETs, naRNA, can engage
209 not only bystander neutrophils in a feed-forward inflammatory response but also other myeloid
210 (monocytes/macrophages) and lymphoid (NK cells) cellular innate immunity. To investigate whether
211 non-hematopoietic cells with immune functions, e.g. tissue cells like keratinocytes, could also
212 respond to RNA-stabilized PMA NETs, N/TERT-1 keratinocytes [27] in monolayers were exposed to
213 PMA-NETs (Fig. 3G). This triggered a dose-dependent IL-8 release comparable to synthetic RNA+LL37,
214 especially under RNA stabilization by RNase inhibitors. Similar results were obtained using primary
215 normal human epidermal keratinocyte (NHEK) monolayers (Fig. 3H). Furthermore, in an 'in vivo'-like
216 human skin equivalent 3D model in which natural keratinocyte differentiation was recapitulated by
217 NHEK cells [28], PMA but not mock NETs significantly induced *IL8* mRNA and protein (Fig. 3I, J). Thus,
218 naRNA can not only activate primary neutrophils in vitro but also trigger broad immune activation in
219 other immune and tissue cells/equivalents.

220 **naRNA displays DAMP activity in vivo in dependence on RNA sensing**

221 Moreover, to gain an insight into whether naRNA could trigger inflammation in vivo in an RNA
222 receptor-dependent manner, we intradermally injected RNase inhibitor-stabilized mock or PMA NETs
223 in the ears of C57BL6 mice. RNA-stabilized PMA NETs were almost as potent to induce ear swelling as
224 synthetic RNA+LL37 (Fig. 4A), but even non-stabilized PMA NETs induced a response significantly
225 higher than mock NETs. The same stimulants were also injected into the ear of *LysM*$^{EGFP/+}$ mice, in
226 which myeloid cells are GFP-positive, thus enabling in vivo monitoring of cellular influx during skin
227 inflammation. Here, RNA-stabilized PMA NETs elicited even greater cellular influx than synthetic
228 RNA+LL37 and mock NETs (Fig. 4B). Importantly, a comparison of WT and *Tlr13*-deficient animals
229 showed that the ear swelling reaction resulting in vivo was naRNA-dependent because RNA-
230 stabilized PMA-NETs were significantly less effective in *Tlr13*-deficient animals (Fig. 4C).

231 **RNA recognition contributes to progressive skin inflammation in experimental psoriasis**

232 Finally, we sought to explore if naRNA was relevant in an animal disease model. The most frequently
233 used murine model of psoriasis uses the TLR7 ligand imiquimod (IMQ) to trigger increasing skin
234 inflammation characterized by epidermal thickening and immune cell infiltration [29]. We previously
235 showed that IMQ treatment also leads to the occurrence of NETs in the tissue [5]. We therefore
236 speculated that naRNA might be involved in disease progression, a hypothesis that could be probed
237 by genetically ablating naRNA sensing and comparing WT and *Tlr13* KO mice. Although in the early
238 induction phase, WT and *Tlr13* KO animals showed a similar increase in ear thickness, the groups
239 diverged from day 3 onwards, after which *Tlr13*-deficient animals were significantly protected from
240 skin inflammation compared to WT mice (Fig. 4D). Additionally, the characteristic epidermal
241 thickening upon IMQ treatment was significantly lower in *Tlr13*-deficient mice compared to WT mice
242 (Fig. 4E, representative image Fig. 4F). The most plausible explanation is that IMQ-initiated NET
243 formation [5] amplifies skin inflammation in WT animals via naRNA, whereas this is prevented in *Tlr13*
244 KO animals. This shows that naRNA can significantly contribute to inflammation in a well-established
245 disease model and can act as a potent inflammation-amplifying endogenous DAMP.

246 Discussion

247 At first sight, it may not seem surprising that the release of NETs, a process that churns up the most
248 critical compartment of a cell, e.g., the nucleus, also inevitably leads to the release of another
249 primary cellular biomolecule, namely RNA. However, independently of whether the process is
250 regulated or not, the release of RNA by NETting PMNs appears to have physiological importance as
251 we have demonstrated here. Rather than acting directly in antimicrobial defense (*cf.* Fig. S2A),
252 naRNA appears to be an LL37-precomplexed DAMP of PMN origin that can be released in the NETting
253 process, and then activates both PMN and other immune and tissue cells in an RNA sensor-
254 dependent manner (Fig. S5). Several further findings warrant further discussion:

255 Firstly, our data revise previous concepts of self-RNA and LL37 in the 'breaking' of innate immune
256 tolerance in psoriasis and the physiological role of NETs in general. naRNA when complexed with
257 LL37, gains stimulatory properties on neutrophils, in line with the existing notion that LL37 may
258 'break' immune tolerance by acting as a physiological 'transfection reagent' for uptake into immune
259 cells, and by shielding it from RNase degradation. However, RNA and LL37 do not appear to
260 aggregate and co-localize 'accidentally' in NETs: quite unexpectedly, they were rather found in even
261 greater co-localization in resting neutrophils, indicating a kind of 'pre-association' and intracellular
262 storage of a pre-defined naRNA-LL37 'composite' DAMP before extrusion during NET formation. It
263 will be interesting to study the process for pre-association for this first 'composite DAMP' and
264 elucidate the precise nature of the RNAs assembled with LL37 in the future Importantly, the
265 identification of such pre-association challenges existing concepts of LL37-RNA complexes as

266 'accidentally assembled' tolerance breakers in certain diseases [7]. Rather, it suggests naRNA-LL37
267 complexes act as purposefully pre-associated DAMPs that arm neutrophils at steady state.
268 Intracellular (rather than accidental/extracellular) pre-association points to a specific role of the
269 naRNA-LL37 DAMP in NET biology and may indicate the NET response to be a DAMP response, rather
270 than an antimicrobial reponse, especially in sterile conditions. Beyond simply amplifying
271 inflammation, we speculate that the physiological relevance of deploying this composite DAMP upon
272 NET formation could be to tag fresh NETs with a timed molecular beacon: Freshly extruded NETs
273 decorated with the naRNA-LL37 DAMP would likely highlight the lingering presence of a pathogenic
274 microorganism or acute tissue damage to other cells not directly engaged by the threat. The naRNA-
275 LL37 DAMP would thus label 'fresh NETs' as 'requiring attention' and triggering further immune
276 activation. Over time, whilst the DNA-related structural and antimicrobial properties of NETs may
277 remain longer, inevitable RNA degradation would lead to deactivation of the composite DAMP,
278 rendering 'old NETs' less immunostimulatory. Further work outside the scope of the present study
279 may explore such a role of naRNA as time-restricted molecular label for NETs.

280 Moreover, our data pertain to the origin and effects of 'extracellular RNA' (exRNA). exRNA is a
281 generic term to indicate a heterogeneous group of RNA molecules which are actively or passively
282 released during sterile inflammation or infectious processes. exRNA can be released in a 'free' state,
283 bound to proteins or phospholipids, in association with extracellular vesicles (EVs) or apoptotic
284 bodies [11]. In all these forms, exRNA may function as a DAMP but also as e.g., procoagulant or
285 regenerative factor [11]. Our data identify naRNA as the first type of exRNA for which a clear
286 physiological origin (NETs) is provided. We speculate that our findings will help trace multiple
287 descriptions of exRNA, on the one side, to neutrophil traps on the other. For example, exRNA has
288 emerged as disease-relevant in atherosclerosis, where it was described to act as a proinflammatory
289 mediator enhancing the recruitment of leukocytes to the site of atherosclerotic lesions as shown in a
290 mouse model of accelerated atherosclerosis [30]. At the same time, NETs have been ascribed a role in
291 amplifying sterile inflammatory responses in an independent mouse model of atherosclerosis by
292 priming macrophages [31]. However, never have these two independent strains of research been
293 connected. By showing NETs to release naRNA, a DAMP type of exRNA, our work connects both lines
294 of enquiry. Likewise, for rheumatoid arthritis (RA), our work makes a plausible link between exRNA in
295 synovial fluid contributing to joint inflammation [32], the emerging role of NETs in RA [33] and even a
296 hitherto enigmatic but therapeutically relevant role of TLR8 [34, 35].

297 Moreover, NETs have been of broad interest focus in COVID-19-related research regarding thrombo-
298 inflammatory states, like sepsis, thrombosis, and respiratory failure, , have been found in plasma of
299 hospitalized COVID-19 patients, and linked to thrombus formation by several research groups [36 37 38
300 39, 40]. Furthermore, exRNAs have been in focus as procoagulant cofactors in blood coagulation [41 42]. A

301 link between NET-related and RNA-induced thrombus formation in COVID-19 has never been made
302 but highlightss naRNA as a potential contributing factor of NET-induced thrombo-inflammatory
303 states in COVID-19 disease pathogenesis. Collectively, we suspect similar links between NETs and
304 exRNA via naRNA to emerge for cardiovascular diseases and cancer if the role of naRNA is thoroughly
305 assessed. Furthermore, the broad sensitivity of immune and tissue cells to naRNA observed by us
306 makes sense of how exRNA may act pathophysiologically.

307 Although we believe PMNs to be the primary trap forming human leukocyte population and hence
308 naRNA the most significant "trap-associated RNA", it will be interesting to explore whether mast cell
309 (MCETs) [43] or macrophage extracellular traps (METs) [44] contain RNA. However, unlike PMN, the latter
310 immune cells are not primary sources of LL37 [17], so that RNA associated with MCETs or METs would
311 be of lesser physiological relevance as a DAMP than naRNA due to a lack of LL37. Therefore,
312 translational approaches, e.g., to restrict trap-RNA mediated amplification of inflammation, should
313 probably center on PMN-derived naRNA. The use of PAD4 inhibitors has already been investigated in
314 animal models to treat cancer or atherosclerotic lesions [45 46] and would represent one potential way
315 of eliminating NETs and hence naRNA-mediated inflammation. However, this would also prevent the
316 effects of NETs that are beneficial for host defense (e.g. physical trapping via DNA and antimicrobial
317 enzymatic activities) and may render treated patients vulnerable to infections. From a translational
318 perspective, our in vivo data indicate that blockade of RNA sensing might be more advantageous,
319 restricting only naRNA mediated responses. Although probably not applicable to patients, it is
320 underscored by evidence that neuroinflammation upon subarachnoid hemorrhage, which is
321 characterized by a NET pathology, is strongly ameliorated by RNase treatment in vivo [47]. More
322 applicable to patients may be the targeting of TLR8 by small molecular antagonists [48] or inhibitory
323 oligonucleotides, which are able to block PMN responsiveness to synthetic RNA in vitro [5]. Exciting is
324 thus the observed efficacy of TLR inhibitory oligoribonucleotides in a psoriasis mouse model [49] and
325 even a first clinical trial in psoriasis patients [50]. We could imagine the blockade of naRNA effects via
326 TLRs highlighted here to emerge as an effective novel strategy to target multiple exRNA or NET-
327 related inflammatory responses.

328 ## Figure legends

329 **Fig. 1**: **naRNA is a canonical component of NETs.**

330 **(A, B)** Confocal microscopy of primary human PMNs stimulated as indicated for 3 h and stained for
331 naRNA (anti-rRNA Y10b, magenta) and DNA (Hoechst 33342, white, n = 3, scale bar: 10 µm,
332 arrowheads point to selected NET strands; representative images in **A**) were quantified in **B** (each dot
333 represents one image, *p<0.05 according to one-way ANOVA). **(C)** Confocal microscopy of primary
334 murine BM-PMNs stimulated as indicated for 16 h and stained as in **A** (n = 3, representative images,
335 scale bar: 10 µm). **(D)** Confocal microscopy of primary human stem cells differentiated *in vitro*
336 with/without 100 µM 5-ethynyluridine (5-EU), click-labeled with a fluorescent dye (yellow, total
337 RNA), anti-rRNA and Hoechst 33342 as in **A** (n = 3, representative images, scale bar: 10 µm, 2 µm in
338 cropped image). **(E)** as in **A** but showing 3D image reconstruction of z-stacks (n = 3, representative
339 images, scale bar: 10 µm). **(F)** Scanning electron microscopy of human primary PMNs treated as
340 indicated and using anti-rRNA primary and immunogold (white arrow)-labeled secondary antibodies
341 and silver enhancement (n = 3, representative images, scale bars as indicated; the two rightmost
342 images show composite images with signals from secondary electron and backscattered electron
343 detectors for topography and additional material information, respectively). **(G)** Agilent TapeStation
344 quantification of naRNA isolated from mock or PMA NETs (from n = 4-6 donors, combined data,
345 mean+SD, each dot represents one biological replicate/donor, *p<0.05 according to Mann-Whitney
346 test). **(H)** RNAseq of PMA NET naRNA (n = 4) and whole PMN RNA (n = 1) (combined data).

347 **Fig. 2. naRNA is a composite DAMP driving NET propagation in human PMN**

348 **(A)** Workflow for NET content preparation from one donor and transfer to naïve human primary
349 PMNs from a second donor. **(B)** Confocal microscopy of primary human PMNs stimulated with NET
350 content harvested with/without RNase inhibitor and diluted 1:50 or 1:500, and then stained for
351 NETs/DNA (Hoechst 33342, n = 9, representative images, scale bar: 10 µm). **(C)** Quantification of **B**
352 using DNA (Hoechst 33342) signal to quantify NET formation (n = 3, combined data, mean+SD, each
353 dot represents one image, *p<0.05 according to one-way ANOVA). **(D)** as in **B** but with/without pre-
354 digestion of NET content with RNase A (n = 3, representative images, scale bar: 10 µm). **(E)**
355 Quantification of **D** (n = 3, combined data, mean+SD, each dot represents the number of NET-positive
356 tiles in one image quantified from three images/condition, *p<0.05 according to one-way ANOVA).
357 **(F)** As in **B** but using purified naRNA (*cf.* Fig. 1G) alone or in complex with exogenously added LL37 (n
358 = 3, representative images, scale bar: 10 µm). **(G)** Confocal microscopy of primary human PMNs
359 stimulated as indicated for 3 h and stained for naRNA (anti-rRNA Y10b, magenta), LL37 (anti-hLL37-
360 DyLight550, yellow), and DNA (Hoechst 33342, white, n = 3, representative images, scale bar 10 µm).
361 **(H)** Pearson's correlation coefficient (colocalization) analysis of **G** (n = 3, combined data, mean+SD,

362 each dot represents one image, three images/condition, *p<0.05 according to one-way ANOVA). **(I)**
363 Line plot analysis of LL37, RNA and DNA staining of unstimulated primary human PMNs of **G** was
364 performed using ZenBlue3 software (n=3, representative graph). **(J)** As in **G**/**I** but on ultrathin
365 sections of unstimulated PMNs (n=3, representative image, scale bar 2 µm). Line plot analysis was
366 performed using ImageJ-Win64 software (n=3, representative graph). **(K)** Transmission electron
367 microscopy of unstimulated human primary PMNs using anti-rRNA and anti-hLL-37 primary and
368 immunogold (6 nm (black arrow) and 12 nm (white arrow) respectively)-labeled secondary
369 antibodies (n = 3, representative images, scale bars as indicated).

370 **Fig. 3. naRNA activity depends on RNA sensors**

371 **(A)** NF-κB dual luciferase assay in HEK293T cell transiently transfected and stimulated as indicated
372 (eV = empty vector, n=3-5, combined data, mean+SD, *p<0.05 according to one-way ANOVA). **(B)**
373 Confocal microscopy of human primary PMNs stimulated as indicated in the presence or absence of
374 CU-CPT9a (100 nM) or Cl-amidine (200 µM, not shown) and stained for NETs/DNA (Hoechst 33342,
375 white, n = 3, representative images, scale bar: 10 µm). **(C)** Quantification of **B** using DNA (Hoechst
376 33342) signal to quantify NET formation (n = 3, combined data, mean+SD, each dot represents the
377 number of NET-positive tiles in one image, three images/condition, *p<0.05 according to non-
378 parametric one-way ANOVA). **(D)** Confocal microscopy analysis of primary C57BL/6 WT or *Tlr13*$^{-/-}$
379 murine BM-PMNs stimulated as indicated and stained for NETs/DNA (Hoechst 33342, white, n = 3,
380 representative images, scale bar: 10 µm). **(E)** Quantification of **D** as in **C** (n = 3, *p<0.05 according to
381 one-way ANOVA). **(F)** Triplicate IL-8 ELISA from WT, *TLR8*$^{-/-}$ and *UNC93B1*$^{-/-}$ BlaER1 macrophage-like
382 cells stimulated as indicated for 18 h (n = 3-4, combined data, mean+SD, each dot represents one
383 biological replicate, *p<0.05 according to one-way ANOVA). **(G)** Triplicate IL-8 ELISA from N/TERT-1
384 keratinocytes stimulated as indicated for 24 h (n = 3, combined data, mean+SD, each dot represents
385 one biological replicate, *p<0.05 according to one-way ANOVA). **(H)** As in **G** but with primary normal
386 human epidermal keratinocytes (NHEK) (n = 3, combined data, mean+SD, each dot represents one
387 biological replicate, *p<0.05 according to one-way ANOVA). **(I, J)** Triplicate relative (to unstimulated)
388 *IL8* mRNA qPCR or IL-8 ELISA from NHEK 3D human skin equivalent constructs stimulated as indicated
389 for 24 h (n = 3, representative of one biological replicate is shown, mean+SD, each dot represents
390 one technical replicate, *p<0.05 according to one-way ANOVA).

391 **Fig. 4. naRNA is a driver of NET-associated *in vivo* inflammation**

392 **(A)** Ear thickness quantified daily in WT C57BL6 mice injected intradermally in vivo on day 0 as
393 indicated (n = 5 per group, combined data, mean+SD, *p<0.05 according to two-way ANOVA). **(B)**
394 Fluorescence imaging monitored hourly in *LysM*$^{EGFP/+}$ mice injected intradermally in vivo at t=0 as
395 indicated (n = 10 per group, combined data, mean+SD, *p<0.05 according to two-way ANOVA). **(C)** As

396 in **A** but also using *Tlr13*$^{-/-}$ mice (n = 7, combined data, mean+SD, *p<0.05 according to two-way
397 ANOVA). **(D)** As in **C** but instead of intradermal injection with topical imiquimod application on day 0–
398 4 (C57BL/6 n = 8, *Tlr13*$^{-/-}$ n = 10, combined data, mean+SD, *p<0.05 according to two-way ANOVA).
399 **(E)** Measurement of epidermal thickness of H&E-stained ear skin specimens of **D** (C57BL/6 n = 8,
400 *Tlr13*$^{-/-}$ n = 10, combined data, mean+SD, *p<0.05 according to Student's *t*-test). **(F)** Histological
401 analysis of H&E-stained ear skin specimens of **E** (C57BL/6 n = 8, *Tlr13*$^{-/-}$ n = 10, representative of one
402 biological replicate is shown, scale bar: 100 µm).

403 **Fig. S1. Controls of IF microscopy, stem cell-derived PMNs, and electron microscopy**

404 **(A)** Confocal microscopy of unstimulated primary human PMNs (control to Fig. 1A) after 3 h and
405 stained for naRNA (anti-rRNA Y10b, magenta) and DNA (Hoechst 33342, white, n = 3, representative
406 images, scale bar: 10 µm). **(B)** Confocal microscopy of unstimulated primary murine BM-PMNs
407 (control to Fig. 1C) after 16 h and stained as in **A** (n = 3, representative images, scale bar: 10 µm). **(C)**
408 Brightfield microscopy analysis of cytospun control primary human stem cell-derived PMNs (control
409 to Fig. 1D) differentiated *in vitro* with/without 100 µM 5-Ethynyluridine (5-EU, n = 3, representative
410 images, scale bar: 20 µm). **(D)** FACS analysis for cells shown in **C** and Fig. 1D (n=3, representative
411 data). **(E)** Scanning electron microscopy of PMA-treated human primary PMNs showing only
412 secondary antibody staining (no primary antibody) control of Fig. 1F (n = 1, representative data; the
413 image on the right is a composite image with signals from secondary electron and backscattered
414 electron detectors for topography and additional material information, respectively).

415 **Fig. S2. Antibacterial effect of NETs on live *S. aureus*, controls of IF microscopy and line plot**
416 **analysis of naRNA and LL37**

417 **(A)** Extracellular bactericidal activity of human PMNs/NETs after infection with *S. aureus* and
418 treatment with RNase A and DNase I during or after formation of PMA-induced NETs (n = 8,
419 combined data, mean+SD, *p<0.05 according to one-way ANOVA). **(B)** Confocal microscopy of
420 unstimulated or PMA-stimulated primary human PMNs (control to Fig. 2B) after 3 h, stained DNA
421 (Hoechst 33342, white, n = 9, representative images, scale bar: 10 µm). **(C)** as in **B** but controls of Fig.
422 2D (n = 3). **(D)** As in **B** but controls of Fig. 2F (n = 3). **(E)** Confocal microscopy of primary human PMNs
423 stimulated as indicated for 3 h and stained for naRNA (anti-rRNA Y10b, magenta), LL37 (anti-hLL37-
424 DyLight550, yellow) and DNA (Hoechst 33342, white, n = 3, representative images). The line plot
425 analysis of LL37, RNA and DNA staining was performed using ZenBlue3 software. Two to three
426 different line plots from the same representative image are shown. **(F)** Transmission electron
427 microscopy of unstimulated human primary PMNs using anti-rRNA and anti-hLL-37 primary and
428 immunogold (6 nm (black arrow) and 12 nm (white arrow) respectively)-labeled secondary
429 antibodies (n = 3, representative images, scale bars as indicated).

430 **Fig. S3. Inhibition of PAD4 in human PMNs during NET formation assay and *Unc93b1*$^{-/-}$ and *Tlr9*$^{-/-}$**
431 **BM-PMN stimulation with human NETs**

432 **(A)** Confocal microscopy of stimulated primary human PMNs after 3 h and stained for DNA (Hoechst
433 33342, white) in the presence or absence of the PAD4-inhibitor Cl-amidine (200 µM, n = 3,
434 representative images; scale bar 10 µm). **(B)** Confocal microscopy of primary C57BL/6 WT or
435 *Unc93b1*$^{-/-}$ murine BM-PMNs stimulated as indicated for 16 h as in **A** (n = 3 WT, n = 1 *Unc93b1*$^{-/-}$,
436 representative images, scale bar: 10 µm). **(C)** Confocal microscopy of primary C57BL/6 WT or *Tlr9*$^{-/-}$
437 murine BM-PMNs stimulated as indicated for 16 h as in **A** (n = 3, representative images, scale bar: 10
438 µm).

439

440 **Fig. S4. Immune responses of PBMCs, macrophages, and NK-cells to NETs and in vivo fluorescence**
441 **imaging**

442 **(A)** Triplicate IL-8 ELISA from WT, *TLR8*$^{-/-}$ and *TLR7*$^{-/-}$ THP-1 cells stimulated as indicated for 18 h,
443 normalized to PMA+ionomycin control (n = 4, combined data, mean+SD, each dot represents one
444 biological replicate, *p<0.05 according to one-way ANOVA). **(B-D)** Triplicate ELISA for TNF (**A**, n = 4),
445 IL-6 (**B**, n = 3), and IL-8 (**C**, n = 3) from primary human PBMCs stimulated as indicated with/without
446 CU-CPT9a for 24 h (combined data, mean+SD, each dot represents one biological replicate, *p<0.05
447 according to one-way ANOVA). **(E)** Triplicate IFN-γ ELISA from NK-92 MI cells stimulated as indicated
448 for 24 h (n = 3, combined data, mean+SD, each dot represents one biological replicate, *p<0.05
449 according to one-way ANOVA).

450 **Fig. S5. Graphical abstract**

451 **Supplemental movie S1: 3D reconstruction of NET DNA network decorated with naRNA**

452 Confocal microscopy of primary human PMNs stimulated with PMA for 3 h, stained for naRNA (anti-
453 rRNA Y10b, magenta) and DNA (Hoechst 33342, white, n = 3) and 3D analysis and animation were
454 performed using ZenBlue3 software.

455 **Supplemental movie S2: Digest of naRNA in PMA-induced NETs**

456 Confocal live microscopy of RNase digestion of NETs obtained from primary human PMNs stimulated
457 with PMA for 3 h, stained for naRNA (SYTO RNAselect, magenta) and DNA (Hoechst 33342, white, n =
458 3). RNase A was added between time point 0 and 5 min (n = 3, scale bar 20 µm). Video analysis and
459 animation were performed using ImageJ-Win64 software.

460

461 **References**

462 1. Brinkmann, V. *et al.* Neutrophil extracellular traps kill bacteria. *Science* **303**, 1532-1535
463 (2004).
464
465 2. Kruger, P. *et al.* Neutrophils: Between host defence, immune modulation, and tissue injury.
466 *PLoS Pathog* **11**, e1004651 (2015).
467
468 3. Boeltz, S. *et al.* To NET or not to NET:current opinions and state of the science regarding the
469 formation of neutrophil extracellular traps. *Cell Death Differ* **26**, 395-408 (2019).
470
471 4. Altincicek, B., Stotzel, S., Wygrecka, M., Preissner, K.T. & Vilcinskas, A. Host-derived
472 extracellular nucleic acids enhance innate immune responses, induce coagulation, and
473 prolong survival upon infection in insects. *J Immunol* **181**, 2705-2712 (2008).
474
475 5. Herster, F. *et al.* Neutrophil extracellular trap-associated RNA and LL37 enable self-amplifying
476 inflammation in psoriasis. *Nat Commun* **11**, 105 (2020).
477
478 6. Lande, R. *et al.* Plasmacytoid dendritic cells sense self-DNA coupled with antimicrobial
479 peptide. *Nature* **449**, 564-569 (2007).
480
481 7. Ganguly, D. *et al.* Self-RNA-antimicrobial peptide complexes activate human dendritic cells
482 through TLR7 and TLR8. *J Exp Med* **206**, 1983-1994 (2009).
483
484 8. Lande, R. *et al.* Cationic antimicrobial peptides in psoriatic skin cooperate to break innate
485 tolerance to self-DNA. *Eur J Immunol* **45**, 203-213 (2015).
486
487 9. Eigenbrod, T. & Dalpke, A.H. Bacterial RNA: An Underestimated Stimulus for Innate Immune
488 Responses. *J Immunol* **195**, 411-418 (2015).
489
490 10. Lind, N.A., Rael, V.E., Pestal, K., Liu, B. & Barton, G.M. Regulation of the nucleic acid-sensing
491 Toll-like receptors. *Nat Rev Immunol* **22**, 224-235 (2022).
492
493 11. Preissner, K.T., Fischer, S. & Deindl, E. Extracellular RNA as a Versatile DAMP and Alarm Signal
494 That Influences Leukocyte Recruitment in Inflammation and Infection. *Front Cell Dev Biol* **8**,
495 619221 (2020).
496
497 12. Schmidt, B. *et al.* Quantification of free RNA in serum and bronchial lavage: a new diagnostic
498 tool in lung cancer detection? *Lung Cancer* **48**, 145-147 (2005).
499
500 13. Zernecke, A. & Preissner, K.T. Extracellular Ribonucleic Acids (RNA) Enter the Stage in
501 Cardiovascular Disease. *Circ Res* **118**, 469-479 (2016).
502
503 14. Lerner, E.A., Lerner, M.R., Janeway, C.A., Jr. & Steitz, J.A. Monoclonal antibodies to nucleic
504 acid-containing cellular constituents: probes for molecular biology and autoimmune disease.
505 *Proc Natl Acad Sci U S A* **78**, 2737-2741 (1981).
506
507 15. Presolski, S.I., Hong, V.P. & Finn, M.G. Copper-Catalyzed Azide-Alkyne Click Chemistry for
508 Bioconjugation. *Curr Protoc Chem Biol* **3**, 153-162 (2011).
509
510 16. Sioud, M. RNA Interference and CRISPR Technologies Technical Advances and New
511 Therapeutic Opportunities Preface. *Methods Mol Biol* **2115**, V-Vii (2020).
512

513 17. Sorensen, O., Arnljots, K., Cowland, J.B., Bainton, D.F. & Borregaard, N. The human
514 antibacterial cathelicidin, hCAP-18, is synthesized in myelocytes and metamyelocytes and
515 localized to specific granules in neutrophils. *Blood* **90**, 2796-2803 (1997).
516
517 18. Colak, E. *et al.* RNA and imidazoquinolines are sensed by distinct TLR7/8 ectodomain sites
518 resulting in functionally disparate signaling events. *J Immunol* **192**, 5963-5973 (2014).
519
520 19. Zhang, S. *et al.* Small-molecule inhibition of TLR8 through stabilization of its resting state. *Nat*
521 *Chem Biol* **14**, 58-64 (2018).
522
523 20. Heil, F. *et al.* Species-specific recognition of single-stranded RNA via toll-like receptor 7 and 8.
524 *Science* **303**, 1526-1529 (2004).
525
526 21. Tabeta, K. *et al.* The Unc93b1 mutation 3d disrupts exogenous antigen presentation and
527 signaling via Toll-like receptors 3, 7 and 9. *Nat Immunol* **7**, 156-164 (2006).
528
529 22. Li, X.D. & Chen, Z.J. Sequence specific detection of bacterial 23S ribosomal RNA by TLR13.
530 *Elife* **1**, e00102 (2012).
531
532 23. Ishii, N., Funami, K., Tatematsu, M., Seya, T. & Matsumoto, M. Endosomal localization of
533 TLR8 confers distinctive proteolytic processing on human myeloid cells. *J Immunol* **193**, 5118-
534 5128 (2014).
535
536 24. Mahdavian Delavary, B., van der Veer, W.M., van Egmond, M., Niessen, F.B. & Beelen, R.H.
537 Macrophages in skin injury and repair. *Immunobiology* **216**, 753-762 (2011).
538
539 25. Vierbuchen, T., Bang, C., Rosigkeit, H., Schmitz, R.A. & Heine, H. The Human-Associated
540 Archaeon Methanosphaera stadtmanae Is Recognized through Its RNA and Induces TLR8-
541 Dependent NLRP3 Inflammasome Activation. *Front Immunol* **8**, 1535 (2017).
542
543 26. Coch, C. *et al.* Human TLR8 Senses RNA From Plasmodium falciparum-Infected Red Blood
544 Cells Which Is Uniquely Required for the IFN-gamma Response in NK Cells. *Front Immunol* **10**,
545 371 (2019).
546
547 27. Dickson, M.A. *et al.* Human keratinocytes that express hTERT and also bypass a p16(INK4a)-
548 enforced mechanism that limits life span become immortal yet retain normal growth and
549 differentiation characteristics. *Mol Cell Biol* **20**, 1436-1447 (2000).
550
551 28. Bitschar, K. *et al.* Lugdunin amplifies innate immune responses in the skin in synergy with
552 host- and microbiota-derived factors. *Nat Commun* **10**, 2730 (2019).
553
554 29. Gilliet, M. *et al.* Psoriasis triggered by toll-like receptor 7 agonist imiquimod in the presence
555 of dermal plasmacytoid dendritic cell precursors. *Arch Dermatol* **140**, 1490-1495 (2004).
556
557 30. Simsekyilmaz, S. *et al.* Role of extracellular RNA in atherosclerotic plaque formation in mice.
558 *Circulation* **129**, 598-606 (2014).
559
560 31. Warnatsch, A., Ioannou, M., Wang, Q. & Papayannopoulos, V. Inflammation. Neutrophil
561 extracellular traps license macrophages for cytokine production in atherosclerosis. *Science*
562 **349**, 316-320 (2015).
563
564 32. Neumann, E., Hasseli, R., Lange, U. & Muller-Ladner, U. The Role of Extracellular Nucleic
565 Acids in Rheumatoid Arthritis. *Curr Pharm Biotechnol* **19**, 1182-1188 (2018).

566
567 33. Song, W., Ye, J., Pan, N., Tan, C. & Herrmann, M. Neutrophil Extracellular Traps Tied to
568 Rheumatoid Arthritis: Points to Ponder. *Front Immunol* **11**, 578129 (2020).
569
570 34. Sacre, S. *et al.* Oligodeoxynucleotide inhibition of Toll-like receptors 3, 7, 8, and 9 suppresses
571 cytokine production in a human rheumatoid arthritis model. *Eur J Immunol* **46**, 772-781
572 (2016).
573
574 35. Sacre, S.M. *et al.* Inhibitors of TLR8 reduce TNF production from human rheumatoid synovial
575 membrane cultures. *J Immunol* **181**, 8002-8009 (2008).
576
577 36. Zuo, Y. *et al.* Neutrophil extracellular traps in COVID-19. *JCI Insight* **5** (2020).
578
579 37. Yaqinuddin, A. & Kashir, J. Novel therapeutic targets for SARS-CoV-2-induced acute lung
580 injury: Targeting a potential IL-1beta/neutrophil extracellular traps feedback loop. *Med*
581 *Hypotheses* **143**, 109906 (2020).
582
583 38. Cicco, S., Cicco, G., Racanelli, V. & Vacca, A. Neutrophil Extracellular Traps (NETs) and
584 Damage-Associated Molecular Patterns (DAMPs): Two Potential Targets for COVID-19
585 Treatment. *Mediators Inflamm* **2020**, 7527953 (2020).
586
587 39. Barnes, B.J. *et al.* Targeting potential drivers of COVID-19: Neutrophil extracellular traps. *J*
588 *Exp Med* **217** (2020).
589
590 40. Golonka, R.M. *et al.* Harnessing innate immunity to eliminate SARS-CoV-2 and ameliorate
591 COVID-19 disease. *Physiol Genomics* **52**, 217-221 (2020).
592
593 41. Kannemeier, C. *et al.* Extracellular RNA constitutes a natural procoagulant cofactor in blood
594 coagulation. *Proc Natl Acad Sci U S A* **104**, 6388-6393 (2007).
595
596 42. Sahu, A. *et al.* MicroRNA-145 Impedes Thrombus Formation via Targeting Tissue Factor in
597 Venous Thrombosis. *EBioMedicine* **26**, 175-186 (2017).
598
599 43. Mollerherm, H., von Kockritz-Blickwede, M. & Branitzki-Heinemann, K. Antimicrobial Activity
600 of Mast Cells: Role and Relevance of Extracellular DNA Traps. *Front Immunol* **7**, 265 (2016).
601
602 44. Doster, R.S., Rogers, L.M., Gaddy, J.A. & Aronoff, D.M. Macrophage Extracellular Traps: A
603 Scoping Review. *J Innate Immun* **10**, 3-13 (2018).
604
605 45. Li, M. *et al.* A Novel Peptidylarginine Deiminase 4 (PAD4) Inhibitor BMS-P5 Blocks Formation
606 of Neutrophil Extracellular Traps and Delays Progression of Multiple Myeloma. *Mol Cancer*
607 *Ther* **19**, 1530-1538 (2020).
608
609 46. Knight, J.S. *et al.* Peptidylarginine deiminase inhibition reduces vascular damage and
610 modulates innate immune responses in murine models of atherosclerosis. *Circ Res* **114**, 947-
611 956 (2014).
612
613 47. Fruh, A. *et al.* RNase A Inhibits Formation of Neutrophil Extracellular Traps in Subarachnoid
614 Hemorrhage. *Front Physiol* **12**, 724611 (2021).
615
616 48. Vlach, J. *et al.* Discovery of M5049: A Novel Selective Toll-Like Receptor 7/8 Inhibitor for
617 Treatment of Autoimmunity. *J Pharmacol Exp Ther* **376**, 397-409 (2021).
618

49. Jiang, W. *et al.* A Toll-like receptor 7, 8, and 9 antagonist inhibits Th1 and Th17 responses and inflammasome activation in a model of IL-23-induced psoriasis. *J Invest Dermatol* **133**, 1777-1784 (2013).

50. Balak, D.M. *et al.* IMO-8400, a toll-like receptor 7, 8, and 9 antagonist, demonstrates clinical activity in a phase 2a, randomized, placebo-controlled trial in patients with moderate-to-severe plaque psoriasis. *Clin Immunol* **174**, 63-72 (2017).

51. Chang, T.-H. *et al.* Transkingdom mechanism of MAMP generation by chitotriosidase (CHIT1) feeds oligomeric chitin from fungal pathogens and allergens into TLR2-mediated innate immune sensing. *bioRxiv*, 2022.2002.2017.479713 (2022).

52. Faust, N., Varas, F., Kelly, L.M., Heck, S. & Graf, T. Insertion of enhanced green fluorescent protein into the lysozyme gene creates mice with green fluorescent granulocytes and macrophages. *Blood* **96**, 719-726 (2000).

53. Bitschar, K. *et al.* Staphylococcus aureus Skin Colonization Is Enhanced by the Interaction of Neutrophil Extracellular Traps with Keratinocytes. *J Invest Dermatol* **140**, 1054-1065 e1054 (2020).

54. Zack, G.W., Rogers, W.E. & Latt, S.A. Automatic-Measurement of Sister Chromatid Exchange Frequency. *Journal of Histochemistry & Cytochemistry* **25**, 741-753 (1977).

Additional information

Author contributions: according to Credit guidelines:

	FB	CGL	CY	SC	YW	MN	JF	JS	PE	MD	KH	BS	SB	MWL	YS
Conceptualization	x														
Data curation															
Formal analysis	x	x	x	x		x	x	x	x		x				
Funding acquisition												x			
Investigation	x	x	x	x		x	x	x	x	x	X				
Methodology											X				x
Project administration					x									X	
Resources													x	X	
Software															
Supervision	X											x			x
Validation	X														
Visualization	x	x	x								X				
Writing: original draft	x														
Writing: review and editing	x	x	x	x	x	x	x	x	x	x	x	x	x	x	x

Conflict of interest statement

NKA has received previous grant support from Pfizer and Boehringer Ingelheim and was a paid consultant for Janssen Pharmaceuticals. All other authors declare no competing interests. S.D.G.

Acknowledgments

650 We gratefully acknowledge Jim Rheinwald, Holger Heine, Austin Chang, Thomas Zillinger for the
651 provision of reagents, respectively, and Jon Kagan and Libera Lo Presti for helpful scientific and
652 editorial comments. We further acknowledge Mark Helm and Martina Christina Schmidt-Dengler for
653 very helpful technical and scientific support. We thank all voluntary healthy donors of biomaterials
654 for participating in the study. The study was supported by the Deutsche Forschungsgemeinschaft
655 (German Research Foundation, DFG) grants CRC TR156 "The skin as an immune sensor and effector
656 organ – Orchestrating local and systemic immunity" (to FB, CG, JF, JS, BS and ANRW), NIH grants
657 R01AI146177, R01AR073665, and R01AR069502 (to NKA). NKA. has received previous grant support
658 from Pfizer and Boehringer Ingelheim and was a paid consultant for Janssen Pharmaceuticals.
659 Infrastructural funding was provided by the University of Tübingen, the University Hospital Tübingen
660 and the DFG Clusters of Excellence "iFIT – Image-Guided and Functionally Instructed Tumor
661 Therapies" (EXC 2180, to AW, PE, BS and MWL), "CMFI – Controlling Microbes to Fight Infection (EXC
662 2124 to AW and BS). Gefördert durch die Deutsche Forschungsgemeinschaft (DFG) im Rahmen der
663 Exzellenzstrategie des Bundes und der Länder - EXC 2180 and EXC 2124. The authors declare no
664 competing financial interests.

665

666 Abbreviations

667 AF – Alexa Fluor; bRNA – bacterial ribonucleic acid; DAMP – damage-associated molecular pattern; 5-
668 EU – 5-Ethynyluridine; FACS – Fluorescence Activated Cell Sorting; fRNA – fungal ribonucleic acid;
669 H&E - Hematoxylin and Eosin; HEK – Human embryonic kidney; HMGB-1 – High-Mobility-Group-
670 Protein B1; HSC – hematopoietic stem cell; IFN – Interferon; IL – Interleukin; KO – knockout; MCET –
671 Mast cell extracellular trap; MET – Macrophage extracellular trap; MPO – Myeloperoxidase; naRNA –
672 Neutrophil extracellular trap-associated RNA; NET – Neutrophil extracellular trap; NK – natural killer;
673 PAD4 - Peptidyl arginine deiminase 4; PBMC - Peripheral Blood Mononuclear Cell; PKC- Protein kinase
674 C; PMN – Polymorphonuclear leukocytes; RT – room temperature; SEM – scanning electron
675 microscopy; TLR – Toll-like receptor; TNF – Tumor necrosis factor

676 ## Materials and Methods

677 **Reagents**

678 PMA (tlrl-pma), Nigericin (tlrl-nig), LL37 (tlrl-l37), as well as the PRR ligands LPS (tlrl-peklps), R848
679 (tlrl-r848), TL8 (tlrl-tl8506), and the TLR8-inhibitor CU-CPT9a (inh-cc9a) were from Invivogen,
680 Ionomycin was acquired from Sigma (I0634-1MG). RNase inhibitor (N2615) was from Promega,
681 RNase A (EN0531), DNase I (EN0521) and DNase inhibitor (EN0521) were from Thermo Fisher. The
682 PAD4-inhibitor Cl-amidine (506282) was from Merck Millipore. DOTAP (L787.2) was from Roth (see
683 Supplementary Table S1), ssRNA40 was from Eurogentec and CpG PTO 2006 from TIB Molbiol (see
684 Supplementary Table S2). Bacterial RNA isolated from *S. aureus* was prepared as described [5]. Fungal
685 RNA from *C. albicans* strain SC5314 was isolated as described below, as well as naRNA isolated from
686 PMA NETs. For complex formation to stimulate cells in a volume of 500 µL, 5.8 µM ssRNA40 (~ 34.4
687 µg/mL), fungal RNA (125 ng/mL), bacterial RNA (10 µg/mL) or PMA NET derived naRNA (~ 600 ng/mL)
688 was mixed with 10 µg LL37 and left for 1 h at room temperature (RT). For a smaller volume of cells,
689 complexes were used in the according fractional amount. For RNA-only or LL37-only controls, the
690 same amounts and volumes were used replacing one of the components with sterile, endotoxin-free
691 H_2O. For complex formation with DOTAP, the according RNA or CpG was incubated with the
692 transfection reagent for 10 min at RT prior to stimulation of the cells. NET content for stimulation
693 was prepared as described below. Antibodies used for fluorescence microscopy, as well as click
694 chemistry reagents are listed in Supplementary Tables S3 and S4. Constructs used for transfection of
695 HEK293T cells are listed in Supplementary Table S5.

696 **Preparation of fungal RNA from *C. albicans***

697 *C. albicans* SC5314 (kindly cultured and prepared by Tzu-Hsuan Chang, Tübingen) was plated in a
698 slant tube containing YPD agar and grown overnight at 30 °C as described in [51]. One colony was
699 picked from the slant tube and resuspended in 500 µL YPD medium, centrifuged at 10,000 rpm for 1
700 min and washed with phosphate-buffered saline (PBS). Afterwards, the pellet was resuspended in
701 200 µL RLT buffer (derived from RNeasy Mini Kit, Qiagen, #74106) and transferred into a 2 mL tube
702 containing 0.5 mm diameter ceramic beads. The tube was filled up to 1 mL with RLT buffer and the
703 fungi were subsequently homogenized by using a microtube homogenizer (BeadBug™, Merck) with
704 an interval of seven times 2 min shaking at 2800 rpm and 1 min cooling break on ice. The
705 supernatant was transferred into a new tube containing 1 mL 75% ethanol (VWR, 20821.330). The
706 further RNA isolation was performed according to the manufacturer's instructions using the Qiagen
707 RNeasy Mini Kit for purification of Total RNA from Animal Tissues (RNeasy Mini Kit, Qiagen, 74106).
708 The RNA was eluted in 30 µL RNase DNase-free H_2O and the concentration was determined with a
709 Nanodrop Spectrophotometer.

710 **Mice**

711 *Unc93b1*$^{3d/3d}$ [21], *Tlr13*$^{-/-}$ [22] (both kindly provided by Tatjana Eigenbrod, Heidelberg and on C57BL/6
712 background) and WT C57BL/6 mice between 8 and 20 weeks of age were used in accordance with
713 local institutional guidelines on animal experiments, regular hygiene monitoring, and specific locally
714 approved protocols compliant with the German regulations of the Gesellschaft für
715 Versuchstierkunde/Society for Laboratory Animal Science (GV-SOLAS) and the European Health Law
716 of the Federation of Laboratory Animal Science Associations (FELASA) for sacrificing and *in vivo* work.
717 *Unc93b1*$^{3d/3d}$, *Tlr13*$^{-/-}$ and WT C57BL/6 control mice were housed in controlled specific-pathogen-free
718 animal facilities at the Interfaculty Institute of Cell Biology, Tübingen. Local federal authority for the
719 approval of experimental protocols was the Regierungspräsidium Tübingen. *Tlr9*$^{-/-}$ mice and matched
720 WT C57BL/6 control mice were a kind gift from Birgit Schittek, Tübingen. LysM$^{EGFP/+}$ [52], *Tlr13*$^{-/-}$ mice [22]
721 (kindly provided by James Chen, Houston and David Nemazee, La Jolla) and WT (all on a C57BL/6
722 background) mouse strains were bred and maintained under the specific pathogen-free conditions,
723 with air isolated cages at an American Association for the Accreditation of Laboratory Animal Care

(AAALAC)-accredited animal facility at Johns Hopkins University and handled according to procedures described in the Guide for the Care and Use of Laboratory Animals as well as Johns Hopkins University's policies and procedures as set forth in the Johns Hopkins University Animal Care and Use Training Manual, and all animal experiments were approved by the Johns Hopkins University Animal Care and Use Committee (MO21M378). Gender-and age-matched 6–8-week-old mice were used for each experiment.

Isolation and stimulation of primary bone-marrow-derived polymorphonuclear neutrophils (BM-PMNs)

Bone-marrow (BM)-PMNs were isolated from the bone marrow as described [5]. In brief, bones were isolated from the respective mice and the bone marrow was flushed out. Afterwards, neutrophils were isolated using magnetic separation (mouse Neutrophil isolation kit, Miltenyi Biotec, 130-097-658) following the manufacturer's instructions. In total, 1×10^5 cells/well PMNs were seeded in a 24-well plate, and stimulation was carried out with PMA (600 nM), ssRNA+LL37 complex (as previously described), nigericin (50 µM), live *C. albicans* (MOI1) or human NET content (mock control and PMA NETs, 1:50 dilution) for 16 h at 37°C and 5% CO2. Subsequently, cells were stained for immunofluorescence.

Study participants and human blood or tissue sample acquisition

All healthy donors included in this study provided their written informed consent before participation. Approval for use of biomaterials was obtained for this project by the local ethics committee of the Medical Faculty Tübingen in accordance with the principles laid down in the Declaration of Helsinki as well as applicable laws and regulations.

Primary human neutrophil isolation and stimulation

Neutrophils of healthy human donors were isolated as described [5]. In brief, EDTA-anticoagulated whole blood was diluted in PBS (Thermo Fisher, 14190-169), loaded on Ficoll (1.077 g/mL, Sigma, 10771) and centrifuged for 25 min at 509 x g at RT without brake. Afterwards, all layers except the erythrocyte-granulocyte layer were discarded and erythrocyte lysis was performed twice (for 20 and for 10 min) using 1x ammonium chloride erythrocyte lysis buffer (see Supplementary Table S6) at 4 °C on roller shaker. The remaining cells were resuspended in culture medium (RPMI culture medium (Sigma-Aldrich, R8758) + 10% FBS (heat-inactivated, sterile filtered, Th. Geyer, 11682258)) to a concentration of 1.6 x 10^6 cells/mL. 500 µL of cells were seeded in a 24-well plate for immunofluorescence microscopy or 8 mL of 5 x 10^6 cells/mL in 10 cm uncoated dishes for NET preparation and naRNA isolation/isolation of whole PMN RNA. After seeding, the cells were rested for 30 min at 37°C and 5% CO_2, followed by 3 h stimulation with PMA (600 nM), nigericin (50 µM), live *C. albicans* (MOI2), RNA+LL37 complexes (as previously described) or NET content at indicated dilutions for IF or 4 h stimulation with PMA (600 nM) for NET preparation. Where indicated, the cells were incubated with 100 nM TLR8-inhibitor CU-CPT9a or 200 µM PAD4-inhibitor Cl-amidine 30 min before stimulation and medium was not replaced during incubation with the respective stimuli.

Primary peripheral blood mononuclear cell (PBMC) isolation and stimulation

PBMCs were isolated from whole blood or buffy coats as described [5]. In brief, EDTA-anticoagulated blood was diluted in PBS and density gradient separation was performed as described above. The PBMC layer was then carefully transferred into another reaction tube and diluted in PBS (1:1). The cell suspension was spun down at 645 × g for 8 min and the cells were washed two more times in PBS and resuspended in culture medium (RPMI + 10% FBS (heat inactivated) +1% L-glutamine) at a density of 1 x 10^6 cells/mL. Afterwards, 200 µL of PBMCs were seeded in a 96-well plate and stimulated with LPS (100 ng/mL), R848 (5 µg/mL), TL8 (100 ng/mL), ssRNA (1.6 µg/mL) + DOTAP (50 µg/mL), ssRNA+LL37 complex (as described above), and respective NET content (1:20 dilution) for 24 h at 37°C and 5% CO_2. Where indicated, the TLR8 inhibitor CU-CPT9a was added to the cells at a concentration of 1 µM 2 h before stimulation and was not removed for the incubation of the cells

772 with the respective stimuli. After the stimulation, the plate was centrifuged for 5 min at 1500 rpm
773 and the supernatant was collected and stored at -80 °C until the ELISA was performed.

774 **Preparation of NETs and isolation of naRNA/whole PMN RNA**

775 NETs were prepared by 600 nM PMA treatment for 4 h at 37°C and 5% CO_2, or cells were left
776 untreated during the incubation as the mock control. After incubation, the neutrophils were gently
777 washed three times with PBS to get rid of PMA as the stimulus for NET formation, any cytokines
778 released by the cells and unstimulated PMNs, as those do not adhere to the uncoated petri dish used
779 here. In some conditions (as indicated) during the NET preparation process and for storage, naRNA
780 was protected by addition of 10 U/µL RNase inhibitor (= mock or PMA NETs + RNase Inhibitor). For
781 digest of NETs, the NET content was incubated for 20 min at 37 °C with RNase A (Thermo Fisher,
782 EN0531; 100 µg/mL, EDTA for DNase inhibition added) at 37 °C. For isolation of naRNA, RNase
783 inhibitor was added to the PMNs during NET formation. After the above-described washing process,
784 PMA or mock NETs were resuspended in 300 µL of ML buffer and RNA isolation was performed
785 according to the manufacturer's instructions (NucleoSpin miRNA isolation kit, Macherey-Nagel,
786 740971.50). The RNA was eluted in 50 µL RNase DNase-free H_2O and the concentration was
787 determined with a Nanodrop Spectrophotometer. For isolation of whole PMN RNA, untreated PMNs
788 were directly lysed, and the RNA was isolated from the cells according to the manufacturer's
789 instructions.

790 **Preparation of human primary stem cell-derived PMNs**

791 Stem cells derived from human healthy donors were prepared and differentiated as described [16]. In
792 brief, bone marrow was diluted in PBS, carefully layered on Ficoll-Paque medium (density: 1.077
793 g/mL) and centrifuged at 500 x g for 25 min at RT without brakes. The interphase layer containing the
794 mononuclear cell fraction was transferred to a new tube and washed twice with 30 mL ice-cold PBS
795 by centrifugation at 300 x g for 8 min at 8 °C. Further, the cells were resuspended, counted, and
796 isolated using Human CD34 MicroBead Kit (Miltenyi) for magnetic beads-based isolation of $CD34^+$
797 cells from BM-MNCs. Afterwards, the number of $CD34^+$ HPSCs was determined and cultured in $CD34^+$
798 culture medium (Stemline II Hematopoietic Stem Cell Expansion medium supplemented with 10%
799 FCS, 1% L-glutamine, 1% penicillin/streptomycin, and a human recombinant cytokine cocktail
800 consisting of 20 ng/mL IL-3, 20 ng/mL IL-6, 20 ng/mL TPO, 50 ng/mL SCF, and 50 ng/mL FLT-3L) at a
801 density of 2 x 10^5/mL at 37 °C and 5% CO_2. The medium was replaced every second day and the cells
802 were cultured for 14 days. During the differentiation process, the cells were treated with 100 µM 5-
803 ethynyluridine for 14 days for subsequent click chemistry labeling of endogenous RNA or were left
804 untreated as negative controls. To verify differentiation, cell morphology was assessed using
805 Cytospin assay. In brief, the Cytoclip™ slide clips were loaded by fitting the filter card, the sample
806 chamber, and the glass slide. An assemble Cytoclip™ slide clip was then placed in the slide clip
807 support plate of the cytospin centrifuge. 2 x 10^4 cells from liquid culture differentiation were
808 pipetted into Cytofunnel™ and centrifuged for 3 min at 200 x g. The cytospin slides were stained for 5
809 min in May-Grünwald stain, rinsed shortly with ddH_2O, and then stained for 10 min in Wright-Giemsa
810 stain. Afterwards, the slides were rinsed shortly with ddH_2O, and cell morphology was determined
811 using a microscope. To further verify differentiation, flow cytometric analysis was performed using
812 antibodies specific for the following hematopoietic/myeloid markers: CD45 (leukocyte marker), CD34
813 (HSPC marker), CD33 (promyelocyte marker), CD11b (myeloid cell marker), CD14 (monocyte marker),
814 and CD15 and CD16 (neutrophil markers). Neutrophil percentage was determined by gating on
815 neutrophils as follows: $CD45^+CD11b^+CD15^+$, or $CD45^+CD11b^+CD16^+$, or $CD45^+CD15^+CD16^+$ cells

816 **BlaER1 cell culture, transdifferentiation and stimulation**

817 BlaER1 cells (WT, *Unc93b*$^{-/-}$ and *Tlr8*$^{-/-}$), a kind gift of Holger Heine, Borstel, Germany [25], were
818 cultured, transdifferentiated, and stimulated for 18 h with the respective stimuli as described [5]. In
819 brief, 1 x 10^6 cells/well were seeded in a 6-well plate and differentiated with 10 ng/mL hIL-3, 10
820 ng/mL hMCSF and 150 nM β-estradiol in complete RPMI-1640 (PANBiotech, P04-18525) for 7 days.
821 Afterwards 5 x 10^4 differentiated cells were reseeded in a 96-well plate, followed by 1 h resting. Cells

822 were treated with the respective stimuli (LPS at 0.1 µg/mL, R848 at 5 µg/mL, TL8 at 100 ng/mL or
823 ssRNA+LL37 complex as described above) and mock or PMA NETs with or without RNase inhibitor) in
824 complete medium in a total volume of 125 µL/well for 18 h. After stimulation, the cells were
825 centrifuged for 5 min at 1200 rpm, the supernatant was transferred into a new plate and stored at -
826 80°C until the ELISA was performed.

827 **THP-1 cell culture, differentiation and stimulation**

828 THP-1 cells (THP-1 cells were a kind gift from Thomas Zillinger, Bonn, Germany [26]), were cultured in
829 complete RPMI-1640 (Sigma, R8758-24X500ML) medium. For differentiation into macrophage-like
830 cells, 5 x 10^4 cells/well were seeded in a 96-well plate, treated with 300 ng/mL PMA and incubated
831 for 16 h at 37°C and 5% CO_2. The next day, the cells were washed three times with PBS and fresh
832 medium was added, followed by 48 h of resting. Subsequently, the medium was removed, exchanged
833 by medium containing 200 U/mL IFN-γ (Sigma, I-3265), and the cells were incubated for 6 h. After
834 repeated washing and medium exchange, cells were treated with the respective stimuli (PMA (25
835 µg/mL) + Ionomycin (0.375 µg/mL), LPS (0.1 µg/mL), R848 (5 µg/mL), TL8 (40 ng/mL), ssRNA+LL37
836 complex (as described above), mock NETs + RNase inhibitor (1:50 dilution), PMA NETs (1:50 dilution)
837 and PMA NETs + RNase inhibitor (1:50 dilution)) in complete medium in a total volume of 125 µL/well
838 for 18 h. After stimulation, the cells were centrifuged for 5 min at 1200 rpm, the supernatant was
839 transferred into a new plate and stored at -80°C until the ELISA was performed.

840 **N/TERT-1 keratinocyte cell culture and stimulation**

841 N/TERT-1 cells (a kind gift from Prof. James Rheinwald [27]) were cultured for less than ten passages in
842 complete CnT-07 medium (CELLnTEC, CnT-07). Two days prior to stimulation, a total amount of 2 x
843 10^4 cells/well was seeded in a 96-well plate and incubated at 37°C and 5% CO_2. The medium was
844 renewed, and the cells were stimulated in a total volume of 125 µL/well of the respective stimuli
845 diluted in medium (PMA (25 µg/mL) + Ionomycin (0.375 µg/mL), TL8 (200 ng/mL), ssRNA+LL37
846 complex (as previously described), as well as mock and PMA NETs with and without RNase inhibitor
847 at indicated dilutions). After 24 h stimulation, the cells were centrifuged at 1200 rpm for 5 min and
848 the supernatant was stored in a new plate at -80°C until further usage.

849 **Primary normal human epidermal keratinocyte (NHEK) cell culture and stimulation**

850 NHEK cells (Normal Human Epidermal Keratinocytes (NHEK) single juvenile donor, proliferating,
851 PromoCell, C-12002) were grown and stimulated in Keratinocyte Growth Medium 2 (PromoCell, C-
852 20111). Two days prior to stimulation, a total amount of 2 x 10^4 cells/well was seeded in a 96-well
853 plate and incubated at 37°C and 5% CO_2. For stimulation, the medium was renewed with basal
854 medium (PromoCell, C-20211) containing 1.7 mM $CaCl_2$ (Roth, CN93.1) and stimuli were added and
855 diluted in medium in a final volume of 125 µL (R848 (20 µg/mL), TL8 (200 ng/mL), ssRNA+LL37
856 complex, as well as mock NETs + RNase inhibitor (1:25 dilution) and PMA NETs with and without
857 RNase inhibitor (1:25 dilution)). After 24 h stimulation, the cells were centrifuged at 1200 rpm for 5
858 min and the supernatant was stored in a new plate at -80°C until further usage.

859 **Preparation of 3D human skin equivalent**

860 The 3D human skin equivalent was prepared as described [53]. Briefly, primary fibroblasts were seeded
861 on collagen and incubated in FF medium for five days. Subsequently, primary keratinocytes were
862 added to the wells and airlifting was performed on day 12. On day 22, the 3D skin model was
863 stimulated with NET content (25 µL/well for one 3D construct grown in a 12-well chamber) or
864 respective water control for 24 h. Afterwards, supernatant was harvested for ELISA, RNA was isolated
865 for qPCR analysis and H&E staining was performed.

866 **NK-92 MI cell culture and stimulation**

867 NK-92 MI cells (kindly provided by Melanie Märklin, University Hospital Tübingen) were cultured in
868 IMDM-Medium (Lonza, 12-722F). For stimulation, a total amount of 1 x 10^5 cells/well were seeded in
869 a volume of 200 µL and rested for 2 h at 37°C and 5% CO_2. The cells were stimulated with LPS (100

870 ng/mL), CpG (2.5 µM) + DOTAP (25 µg/mL), R848 (5 µg/mL), TL8 (100 ng/mL), ssRNA (1.6 µg/mL) +
871 DOTAP (50 µg/mL), ssRNA+LL37 complex (as described above), or NET content (1:100 dilution) for 24
872 h and afterwards centrifuged for 5 min at 1500 rpm. Subsequently, the supernatant was transferred
873 into a new plate and stored at -80°C until further usage.

874 **Flow cytometry**

875 After PMN isolation, the purity and activation status of the cells was determined by flow cytometry
876 as described [5]. In brief, 200 µL of cells were transferred into a 96-well plate (U-bottom) and
877 centrifuged for 5 min at 448 x g. Afterwards, blocking was performed using pooled human serum
878 diluted 1:10 in PBS for 15 min at 4°C. After washing, the samples were stained for 20 min at RT in
879 the dark and fixed (4% PFA in PBS) after repeated washing for 10 min at RT in the dark. After an
880 additional washing step, the cell pellets were resuspended in 300 µL PBS and measurements were
881 performed on a FACS Canto II (BD Bioscience, Diva software). Analysis was performed using FlowJo
882 V10 analysis software.

883 **RNA sequencing analysis of naRNA**

884 Isolated naRNA was analyzed for quality control using the Agilent 4200 TapeStation system.
885 Subsequently, the RNA was sequenced according to NEBNext® Ultra™ II Directional RNA Library Prep
886 Kit for Illumina® using the protocol for use with rRNA Depleted FFPE RNA. The data was quantified
887 using Salmon Version1.5.0 and tximport was used to obtain the transcript-level quantification. For
888 transcript classification, GENECODE annotation was performed.

889 **Fluorescence microscopy of fixed human or murine primary neutrophils**

890 500 µL of 1.6 x 10^6 cells/mL of human blood PMNs, and 2 x 10^6 cells/mL murine BM-PMNs were
891 seeded in a 24-well plate containing poly-L-lysine-coated glass coverslips (Electron Microscopy
892 Sciences, 72292-04) and rested for 30 min before stimulation at 37°C and 5% CO_2 with the according
893 stimuli (as described above) for 3 h (human) or 16 h (murine), respectively, as adapted from
894 Brinkmann *et al.*, 2004 [1]. After stimulation, the cells were carefully washed with PBS and fixed with
895 fixation buffer (Biolegend, 420801) for 10 min at RT in the dark. Afterwards, the cells were blocked
896 with PBS containing 0.1% heat-inactivated diethylpyrocarbonate (DEPC) (Roth, K028.2), 10% chicken
897 serum (Normal Chicken Serum Blocking Solution S-3000, Biozol/Vectorlabs, VEC-S-3000-20), 0.1%
898 saponin (Applichem, A4518.0100), as well as 10 U/µL RNase inhibitor for 2 h at RT. The primary
899 antibodies (rRNA Y10b, hLL37, see Supplementary Table S3) were diluted 1:50 in blocking buffer and
900 subsequently incubated for 2 h at RT. Afterwards, the cells were washed three times with PBS
901 containing 0.1% heat inactivated DEPC and incubated with the secondary antibodies (see
902 Supplementary Table S3) in a 1:500 dilution in blocking buffer for 1 h. After repeated washing, the
903 cells were incubated with Hoechst 33342 (Thermo Fisher; 1 µg/mL) for 5 min to stain nuclear DNA.
904 Secondary antibodies alone did not yield any significant staining under identical staining and
905 acquisition conditions. The coverslips were mounted (ProLong™ Diamond Antifade Mountant,
906 Thermo Fisher, P36961) on glass slides and left to dry overnight at RT in the dark. Subsequently, the
907 samples were stored at 4°C before microscopy using a Zeiss LSM800 Confocal microscope (40x or 63x
908 magnification with z-stack acquisition, AiryScan mode) and image analysis using ImageJ-Win64 and
909 Zen Blue3 software was performed. For IF of ultrathin sections, coverslips were coated with a carbon
910 layer, glow-discharged and UV-treated overnight before cells were seeded. After incubation, the cells
911 were fixed in 2.5% glutaraldehyde in PBS for 2 h at room temperature followed by incubation at 4°C.
912 Samples were prepared by the progressive lowering of temperature method (PLT). Therefore, the
913 fixed cells were incubated in ethanol for infiltration of Lowicryl HM20, followed by UV polymerization
914 and subsequent sectioning into 50-60 nm ultrathin slices. Immunolabeling was performed by
915 incubation with anti-rRNA Y10b and anti-LL37 primary antibodies for 1 h at RT. Afterwards, the cells
916 were incubated with goat anti-mouse Cy3 and goat anti-rabbit AF488 in blocking buffer for 1 h at RT.
917 Following immunolabeling, the samples were treated with 1% uranyl acetate for 5 min at RT before
918 analysis using a Zeiss Axioplan microscope (63x objective, Olympus SIS cell software) and image/line
919 plot analysis was performed using ImageJ-Win64.

920 **Quantification of NET formation**

921 To quantify the formation of NETs, microscopy images were obtained using a Zeiss LSM800 Confocal
922 microscope with a 40x objective and 3x3 tiles acquisition. Three images per sample of three
923 biological replicates were taken. To quantify NET formation by using NET-related signal dispersion of
924 rRNA and DNA signal, ImageJ-Win64 software was used, and a threshold (Triangle threshold) was
925 applied as originally described [54]. Particles were analyzed with a ROI (region of interest) manager
926 (size (micron^2): 100-infinity (pixel units); circularity 0.00-1.00) and average size and number of
927 particles (ROIs) were assessed. In NETs, RNA and DNA signals showed up in a greater number and
928 smaller size, making the usage of the ratio suitable as a measurement of NET-related signal
929 dispersion. In the case of using the DNA signal only to assess NET formation, ImageJ-Win64 software
930 was used to create a PNG image and a grid with 8x8 tiles was manually applied to the images. Tiles
931 containing extracellular DNA structures were manually counted in a blinded manner as NET-positive
932 tiles.

933 **Live fluorescence microscopy of enzymatic digest of human NETs**

934 500 µL of 1.6 x 10^6 cells/mL of human blood PMNs were seeded in a 4-well glass bottom microscopy
935 cell culture dish (Greiner, 627871) and rested for 30 min before stimulation at 37°C and 5% CO_2 with
936 PMA (600 nM) for 3 h. After stimulation, the medium was carefully removed and the cells were
937 washed with PBS before adding fresh culture medium (RPMI culture medium without phenol red
938 (Sigma-Aldrich, R7509)+10% FBS (heat inactivated, sterile filtered, TH Geyer, 11682258)). Hoechst
939 33342 (Thermo Fisher, 1 µg/mL) to stain nuclear DNA and SYTO RNAselect Green fluorescent dye
940 (Thermo Fisher, 50 µM) to stain naRNA was added to the cells, as well as RNase A (Thermo Fisher,
941 EN0531; 100 µg/mL) was added between time point 0 and 5 min. Live cell imaging was performed
942 using a Zeiss LSM800 Confocal microscope with a 63x objective and z-stack acquisition, taking an
943 image every 5 min for 30-60 min respectively. Image analysis and video creation was performed
944 using ImageJ-Win64.

945 **Click chemistry of primary, stem cell-derived PMNs and fluorescence microscopy**

946 500 µL of 1.6 x 10^6 cells/mL of human stem cell-derived PMNs treated with 5-ethynyluridine or left
947 untreated were seeded in a 24-well plate containing poly-L-lysine-coated glass coverslips and rested
948 for 30 min before stimulation with PMA (600 nM) at 37°C and 5% CO_2 for 12 h. After stimulation, the
949 cells were washed and permeabilized with ice-cold acetone (Applichem, A1582.2500PE) 1:1
950 methanol (Honeywell, 32213-2.5L) for 5 min at RT. Subsequently, the click chemistry (reagents see
951 Supplementary Table S4) labeling of endogenous RNA was performed as described [15]. Briefly, in a
952 total volume of 500 µL, 2 µL of AF546-Azide, a pre-mixture of 1 mM $CuSO_4$ and 1.25 mM THPTA, 5
953 mM aminoguanidine-hydrochloride and 5 mM Na-ascorbate in PBS were added to the cells in a 24-
954 well plate. The wells were sealed with plastic foil and incubated for 1 h at RT while shaking in the
955 dark. For negative controls, 5-ethynyluridine untreated cells incubated with complete click chemistry
956 reagents and 5-ethynyluridine treated cells incubated with PBS and AF546-Azide only were used. No
957 significant signals were observed. After the incubation, the cells were washed three times for 5 min
958 with PBS and counterstained with rRNA Y10b-AF647 (see Supplementary Table S3) at 1:50 in PBS for
959 2 h at RT in the dark. After repeated washing, the cells were incubated with Hoechst 33342 to stain
960 nuclear DNA and mounted as described above. Imaging and analysis were performed as previously
961 described.

962 **Electron microscopy**

963 For electron microscopy, 500 µL of 1.6 x 10^6 cells/mL of human blood-derived PMNs were seeded in a
964 24-well plate containing coverslips which were pre-coated with 0.01 % poly-L-lysine (Sigma, A-005-C)
965 for 15 min at 37°C for scanning electron microscopy (SEM). For transmission electron microscopy
966 (TEM), coverslips were coated with a carbon layer, glow-discharged and UV-treated overnight before
967 cells were seeded. Cells were rested for 30 min at 37°C and 5% CO_2 and subsequently stimulated with
968 1200 nM PMA or left untreated for 3 h. Afterwards, the cells were fixed in 2.5% glutaraldehyde in

969 PBS for 2 h at room temperature followed by incubation at 4°C. For SEM, samples were post-fixed
970 with 1% osmium tetroxide for 1 h on ice. Subsequently, samples were dehydrated in a graded
971 ethanol series followed by critical point drying (CPD300, Leica Microsystems) with CO_2. Finally, the
972 cells were sputter-coated with a 4 nm thick layer of platinum (CCU-010, Safematic) and examined
973 with a field emission scanning electron microscope (Regulus 8230, Hitachi High Technologies) at an
974 accelerating voltage of 3 kV. For antibody labeling, cells treated as described above were fixed in 4%
975 formaldehyde in PBS for 1-2 hours at room temperature and 4°C overnight. After washing and
976 blocking (0.2% gelatin in PBS) samples were incubated for 1 h at room temperature with rRNA Y10b
977 as the primary antibody in blocking buffer and for 1 h at RT with goat anti-mouse antibodies coupled
978 to 6 nm gold in blocking buffer (Jackson ImmunoResearch, code number 115-195-166). Samples
979 labeled with 6 nm gold were further silver enhanced. Following immunolabeling, the samples were
980 treated with 1% uranyl acetate for 5 min at RT, dehydrated and critical point dried as before.
981 Samples were sputter-coated with a 5 nm thick layer of carbon (CCU-010, Safematic) and analyzed in
982 the SEM with an accelerating voltage of 5 kV. For TEM, samples were prepared by the PLT method as
983 described above for IF of ultrathin sections. Samples were placed on grids (Cu, Ni) and subsequently
984 sectioned into 50-60 nm ultrathin slices. Immunolabeling was performed by incubation with anti-
985 rRNA Y10b as the first primary antibody in blocking buffer at 4°C overnight, followed by incubation
986 with anti-LL37 as the second primary antibody for 1 h at RT. Afterwards, the cells were incubated
987 with goat anti-mouse coupled to 6 nm gold and goat anti-rabbit 12 nm gold secondary antibodies in
988 blocking buffer for 1 h at RT. Following immunolabeling, the samples were treated with 1% uranyl
989 acetate for 5 min at RT before analysis in the TEM.

990

991 **Transient transfection of HEK293T cells**

992 HEK293T cells were transiently transfected with the respective TLR8, TLR7, TLR9 and NF-κB reporter
993 plasmids as described [18] (see Supplementary Table S5 for plasmids) using X-tremeGENE™ HP DNA
994 Transfection Reagent (Merck, 6366236001). A total amount of 5 x 10^4 cells/well were seeded in a 24-
995 well plate one day prior to transfection. For the transfection of one well, 100 ng of the according TLR
996 plasmid, 100 ng of the firefly luciferase NF-κB reporter and 10 ng *Renilla* luciferase control reporter
997 was mixed in Opti-MEM™ Reduced Serum Medium (Thermo Fisher, 31985062) in a total volume of
998 50 µL. After 15 min incubation at RT, the transfection mix was added to the cells and the cells were
999 incubated for 48 h. Prior to subsequent stimulation, the medium was changed to complete DMEM
1000 medium (Sigma, D5796-24X500ML), and the cells were incubated with the respective NET content
1001 stimuli and controls (R848 (2.5 µg/mL), TL8 (100 ng/mL), CpG (1.25 µM) + DOTAP (25 µg/mL), ssRNA
1002 (0.6 µg/mL) + DOTAP (20 µg/mL), mock NETs + RNase inhibitor (1:50 dilution), PMA NETs (1:50
1003 dilution), PMA NETs + RNase inhibitor (1:50)) for 18 h at 37°C and 5% CO_2. Supernatants were then
1004 removed, and the cells frozen briefly at -80 °C. Subsequently they were used for dual luciferase assay.

1005 **Dual luciferase reporter assay**

1006 The dual luciferase reporter assay for detection NF-κB activation after TLR transfection and
1007 subsequent stimulation was performed as described [5]. In brief, supernatants were removed from the
1008 cells after stimulation and 60 µL/well of 1x passive lysis buffer (E194A, Promega) was added. The
1009 plate was then incubated for 15 min at RT on the plate shaker and subsequently stored at −80°C for
1010 at least 15 min to facilitate complete cell lysis. After thawing, the cell solution (60 µL) was
1011 transferred into a V-bottom 96-well plate and centrifuged for 10 min at 2500 rpm and 4°C to pellet
1012 cell debris. Ten microliters of supernatant were then transferred into a white microplate and each
1013 condition was measured in triplicates using the FLUOstar OPTIMA device (BMG Labtech). Firefly and
1014 Renilla luciferase activity were determined using the Promega Dual luciferase kit. Both enzyme
1015 activities were measured for 12.5 s with 24 intervals of 0.5 s, respectively. The data was analyzed by
1016 calculating the ratio of the two measured signals, thereby normalizing each firefly luciferase signal to
1017 its corresponding Renilla luciferase signal. The ratios were represented as the relative light units
1018 (RLU) of NF-κB activation.

1019 **Extracellular bacterial killing of *S. aureus***

1020 The killing assay of *S. aureus* with human PMNs was performed according to Brinkmann *et al.*, 2004 [1].
1021 In brief, PMNs were seeded at a density of 2 x 10^6 cells/mL and incubated with PMA (600 nM) for 2 h
1022 at 37°C. Afterwards, the medium was carefully replaced with serum-free culture medium, containing
1023 2% heat-inactivated pooled human serum with cytochalasin D (10 µg/mL) and incubated further for
1024 15 min before infection with bacteria. Cytochalasin D treatment did not affect NETs and this
1025 concentration was effective in blocking bacterial phagocytosis. To investigate whether naRNA of
1026 NETs was important in extracellular killing, samples were either treated with RNase A (Thermo
1027 Fisher, EN0531; 100 µg/mL) or DNase I (Thermo Fisher, EN0521; 1 U/10 µL) for 2 h during NET
1028 formation, or after NET formation during the 30 min bacterial killing process. Samples were
1029 centrifuged at 700 x g for 10 min and incubated at 37°C and 5% CO_2 for 30 minutes. Bacterial killing
1030 was measured as percentages of control values (bacteria incubated alone in media without
1031 neutrophils).

1032 **In vivo analysis of naRNA DAMP effects**

1033 To investigate the effect of NETs with or without RNase inhibitors and the respective TLR signaling,
1034 20 µL of NET content and the respective controls were injected into the ears of C57BL/6 and *Tlr13*$^{-/-}$
1035 mice intradermally on day 0. Afterwards, as a measure of inflammation, the ear thickness was
1036 assessed using a manual caliper (0.01–10 mm, Peacock, Tokyo, Japan) until day 4.

1037 **Neutrophil infiltration *in vivo* fluorescence imaging**

1038 The *in vivo* experiment for investigating neutrophil infiltration was performed as described [5]. Briefly,
1039 LysM$^{EGFP/+}$ mice were injected intradermally with 20 µL of PMA or mock NET content or respective
1040 controls. LysM$^{EGFP/+}$ mice were then anesthetized with inhalation isoflurane and *in vivo* fluorescence
1041 imaging was performed using the IVIS Lumina II imaging system (Caliper). EGFP fluorescence was
1042 measured using excitation (465 nm), emission (515–575 nm), and exposure time (0.5 s). Data are
1043 quantified as total radiant efficiency ([photons/s]/[µW/cm^2]) within a circular region of interest using
1044 Living Image software (Caliper).

1045 **Imiquimod model of psoriatic skin inflammation**

1046 To analyze the effect of RNA signaling in an *in vivo* model for psoriasis, the well-established
1047 imiquimod mouse model was used [29]. C57BL/6 and *Tlr13*$^{-/-}$ mice were used and, briefly, 70 µL (62.5
1048 mg) of imiquimod (5%, Taro Pharmaceuticals Industries, Hawthorne, NY) was applied daily to both
1049 sides of a mouse ear for 5 consecutive days (day 0 to 4). Ear thickness was measured with a manual
1050 caliper (0.01–10 mm, Peacock, Tokyo, Japan) before imiquimod application. A day after the last
1051 application of imiquimod (day 5), full-thickness ear skin was excised with surgical scissors for
1052 histologic analysis.

1053 **Histologic analysis of mouse ear skin**

1054 Ear skin specimens were collected by excising the entire ear with surgical scissors, fixed in formalin
1055 (10%), and embedded in paraffin. 4 µm thickness sections were mounted onto glass slides and
1056 stained with H&E by the Johns Hopkins Reference Histology Laboratory. To measure epidermal
1057 thickness, 100 epidermal thickness measurements per mouse were averaged from images taken at
1058 ×200 magnification (Hamamatsu Nanozoomer) using ImageJ software (NIH).

1059 **ELISA**

1060 To measure cytokine release of BlaER-1, THP-1, N/TERT-1, NHEK, NK-92 MI, PBMCs and 3D human
1061 skin equivalent after stimulation with NET content and respective controls, ELISA Kits for hIL-8 (ELISA
1062 MAX™ Deluxe Set Human IL-8, Biolegend, 431504), hIL-6 (ELISA MAX™ Deluxe Set Human IL-6,
1063 Biolegend, 430504), IFN-γ (ELISA MAX™ Deluxe Set Human IFN-γ, Biolegend, 430104), and TNF (TNF
1064 alpha Human Uncoated ELISA Kit, Invitrogen, 88-7346-88) were used according to the manufacturer's
1065 instructions. Samples were assessed in triplicates.

1066 **qPCR analysis of IL-8 expression of 3D human skin equivalent**

1067 To investigate IL-8 expression of 3D human skin equivalent after stimulation with NET contents, qPCR
1068 analysis was performed. First, total RNA was isolated using the RNeasy Mini Kit (Qiagen, 74106) for
1069 animal tissues and cells. For cDNA preparation, the High-Capacity RNA-to-cDNA-Kit (Thermo Fisher,
1070 4387406) was used according to the manufacturer's instructions. For the qPCR, the TaqMan™ system
1071 was used. Briefly, a master mix of TaqMan™ Universal Mastermix II (Thermo Fisher, 4440040) and
1072 TaqMan™ Gene Expression Assay (Thermo Fisher, 4448892) was prepared according to the
1073 manufacturer's instructions. For one reaction, 5.5 µL master mix and 4.5 µL of the respective cDNA
1074 (IL-8 and TBP) were mixed and the qPCR was run. Analysis in triplicates was performed using
1075 QuantStudio Real-Time-PCR software version 1.3 (Thermo Fisher).

1076 **Statistics**

1077 Experimental data were analyzed using Excel 2019 (Microsoft) and/or GraphPad Prism 8, microscopy
1078 data with ImageJ-Win64 or ZenBlue3 software, flow cytometry data with FlowJo V10. Normal
1079 distribution in each group was always tested using the Shapiro–Wilk test first for the subsequent
1080 choice of a parametric (ANOVA, Student's t-test for normally distributed data) or non-parametric
1081 (Mann–Whitney U) test as indicated in figure legelnds. p-values ($\alpha = 0.05$) were then calculated, and
1082 multiple testing was corrected for in Prism, as indicated in the figure legends. Values < 0.05 were
1083 generally considered statistically as significant and denoted by * throughout even if considerably
1084 lower. Comparisons made to unstimulated control, unless indicated otherwise, were denoted by
1085 brackets.

1086 **Supplementary Tables**

1087 **Supplementary Table 1: commercial TLR ligands and inhibitors; enzymes**

Component	Company	Product no.
Cl-amidine	Merck	506282
CpG PTO 2006	TIB Molbiol	n/a, see Table S2
CU-CPT9a	Invivogen	inh-cc9a
DNase I	Thermo Fisher	EN0521
DNase inhibitor 50 mM EDTA	Thermo Fisher	EN0521
DOTAP	Roth	L787.2
Ionomycin	Sigma	I0634-1MG
LL37	Invivogen	tlrl-ll37
LPS-EK (ultrapure)	Invivogen	tlrl-peklps
Nigericin	Invivogen	tlrl-nig
PMA	Invivogen	tlrl-pma
R848 (Resiquimod)	Invivogen	tlrl-r848
RNase A	Thermo Fisher	EN0531
RNase inhibitor	Promega	N2615
TL8-506	Invivogen	tlrl-tl8506

1088

1089 **Supplementary Table 2: Nucleic acid TLR agonists**

Component	Sequence	Backbone	Company
RNA40	5'GsCsCsCsGsUsCsUsGsUsUsGsUsGsUsGsAsCsUsC3'	Phosphorothioate	Eurogentec
CpG PTO 2006	5'TsCsGsTsCsGsTsTsTsTsGsTsCsGsTsTsTsTsGsTsCsGsTsT3'	Phosphorothioate	TIB

1090

1091 **Supplementary Table 3: Antibodies and conjugation kit**

Item	Fluorophore	Species	Isotype	Company	Product no.
Anti-hLL37	DyLight 550	rabbit	IgG	LSBio	LS-B6696-500
DyLight 550 Conjugation Kit (Fast)	DyLight 550	-	-	Abcam	ab201800

Anti-rRNA (Y10b)	unconjugated	mouse	IgG_{2a} κ	Santa Cruz Biotechnology	sc-33678
Anti-rRNA (Y10b) Alexa Fluor® 647	AF647	mouse	IgG_{2a} κ	Santa Cruz Biotechnology	sc-33678 AF647
Anti-mouse IgG	AF647	chicken	IgY	Thermo Fisher	A-21463
Hoechst 33342	-	-	-	Thermo Fisher	H21492
SYTO RNAselect Green fluorescent dye	-	-	-	Thermo Fisher	S32703
Anti-mouse Cy3	Cy3	goat	IgG	Jackson ImmunoResearch	115-165-146
Anti-rabbit AF488	AF488	goat	IgG	Molecular Probes	A-11008
Anti-mouse 6 nm gold	-	goat	IgG	Jackson ImmunoResearch	115-195-166
Anti-rabbit 12 nm gold	-	goat	IgG	Jackson ImmunoResearch	111-205-144

1092

1093 **Supplementary Table 4: Click chemistry reagents**

Reagent	Company	Product no.
AF546-Azide	Jena Bioscience	CLK-1283-1
Aminoguanidine-Hydrochloride	Merck	396494-25G
$CuSO_4$-click chemistry grade	Jena Bioscience	CLK-MI004-50.1
5-Ethynyluridine	Jena Bioscience	CLK-N002-10
Na-Ascorbate-click chemistry grade	Jena Bioscience	CLK-MI005-1G
THPTA (Tris((1-hydroxy-propyl-1H-1,2,3-triazol-4-yl)methyl)amine)	Jena Bioscience	CLK-1010-25

1094

1095 **Supplementary Table 5: Plasmids used for HEK293T transfection**

Plasmid name insert	Vector backbone	Insert
NF-κB reporter	pGL3	6x NF-κB response element
Renilla	pRL-TK	*Renilla*
hTLR7	pcDNA3.1 (+)	hTLR7
hTLR8	pcDNA3.1 (+)	hTLR8
hTLR9	pSEM-hTLR9	hTLR9

1096

1097 **Supplementary Table 6: primers used for qPCR**

Gene	Assay number
IL-8	Hs00174103_m1
TBP (housekeeper)	HS00427620_m1

1098

1099 **Supplementary Table 7: 10x Ammonium chloride erythrocyte lysis buffer**

Compound	Company	Product no.
1.54 M NH_4Cl	Roth	5470.1
100 mM $KHCO_3$	Fluka	60220
1 mM EDTA; pH 8 dissolved in Ampuwa water	Thermo Fisher Fresenius Kabi	15575020 1833
pH adjusted to 7.3, sterile filtered (0.22 µm)		

1100

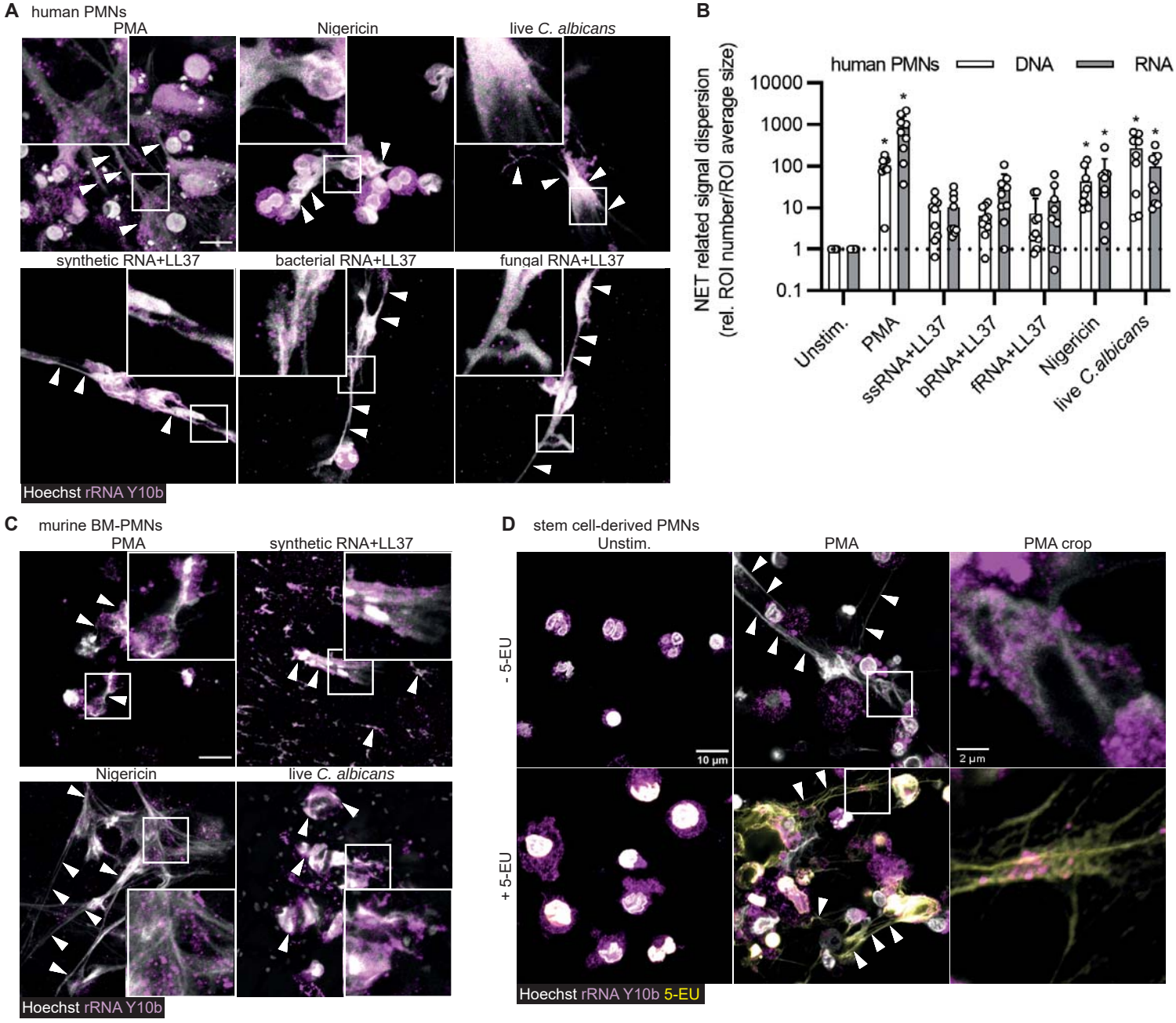
A human PMNs
PMA
Nigericin
live C. albicans
synthetic RNA+LL37
bacterial RNA+LL37
fungal RNA+LL37
Hoechst rRNA Y10b
B
human PMNs
DNA
RNA
NET related signal dispersion (rel. ROI number/ROI average size)
10000
1000
100
10
1
0.1
Unstim.
PMA
ssRNA+LL37
bRNA+LL37
fRNA+LL37
Nigericin
live C.albicans
C murine BM-PMNs
PMA
synthetic RNA+LL37
Nigericin
live C. albicans
Hoechst rRNA Y10b
D stem cell-derived PMNs
Unstim.
PMA
PMA crop
- 5-EU
+ 5-EU
10 µm
2 µm
Hoechst rRNA Y10b 5-EU
E human PMNs
10 µm
1 µm
Hoechst rRNA Y10b
G
NET derived RNA
naRNA (ng/µL)
80
60
40
20
0
Mock
PMA
H
RNA-Seq
RNA types (%)
100
75
50
25
0
whole RNA
naRNA
unknown
rRNA
ncRNA
nonsense mediated decay
altern. spliced transcript
pseudogene
mRNA
F human PMNs
Unstim.
PMA
200 µm
20 µm
200 µm
5 µm
1 µm

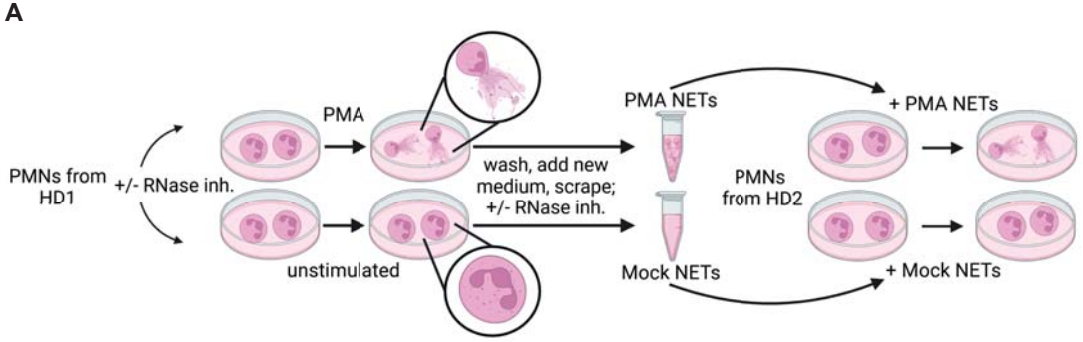
A
PMNs from HD1
+/- RNase inh.
PMA
unstimulated
wash, add new medium, scrape; +/- RNase inh.
PMA NETs
Mock NETs
PMNs from HD2
+ PMA NETs
+ Mock NETs

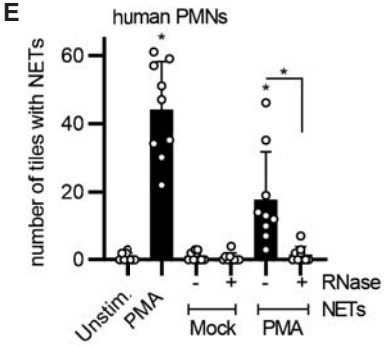
E
human PMNs
number of tiles with NETs
60
40
20
0
RNase
NETs
Unstim.
PMA
Mock
PMA

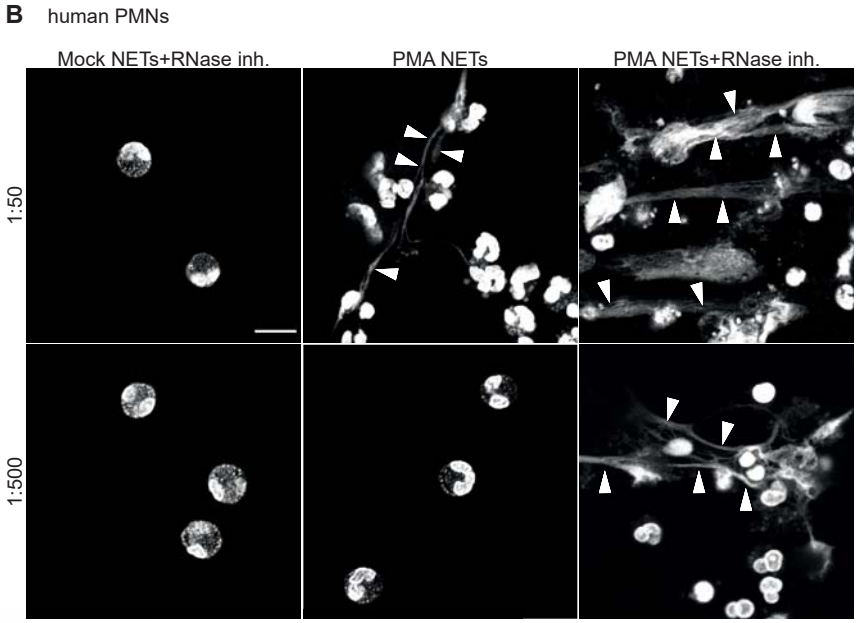
B
human PMNs
Mock NETs+RNase inh.
PMA NETs
PMA NETs+RNase inh.
1:50
1:500

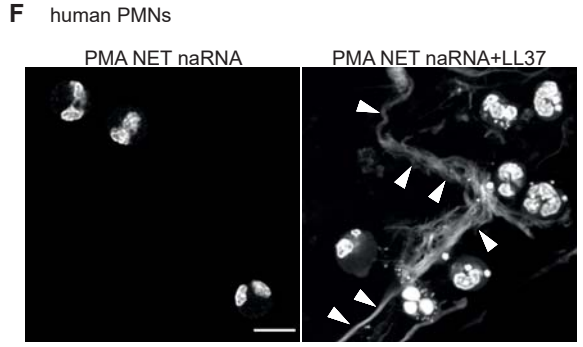
F
human PMNs
PMA NET naRNA
PMA NET naRNA+LL37

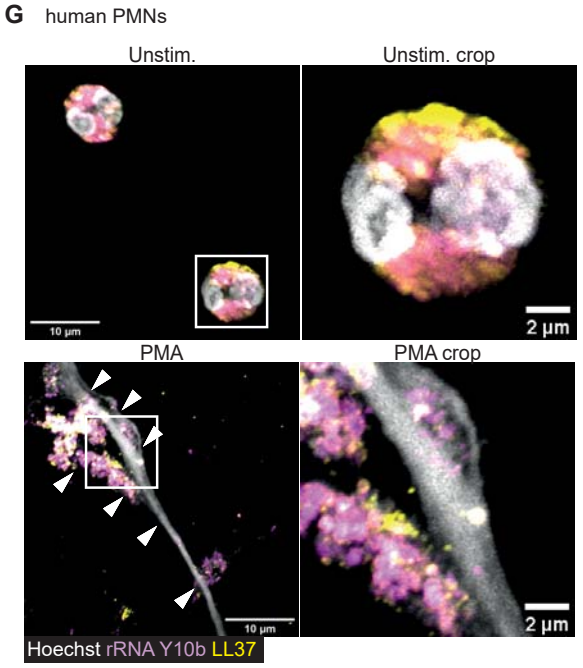
G
human PMNs
Unstim.
Unstim. crop
10 µm
2 µm
PMA
PMA crop
10 µm
2 µm
Hoechst rRNA Y10b LL37

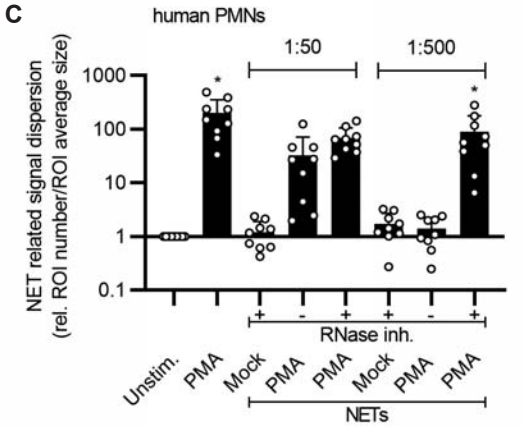
C
human PMNs
1:50
1:500
NET related signal dispersion
(rel. ROI number/ROI average size)
1000
100
10
1
0.1
RNase inh.
Unstim.
PMA
Mock
PMA
PMA
Mock
PMA
PMA
NETs

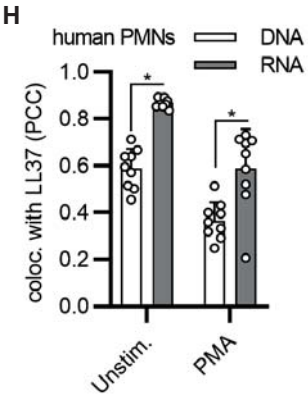
H
human PMNs
DNA
RNA
coloc. with LL37 (PCC)
1.0
0.8
0.6
0.4
0.2
0.0
Unstim.
PMA

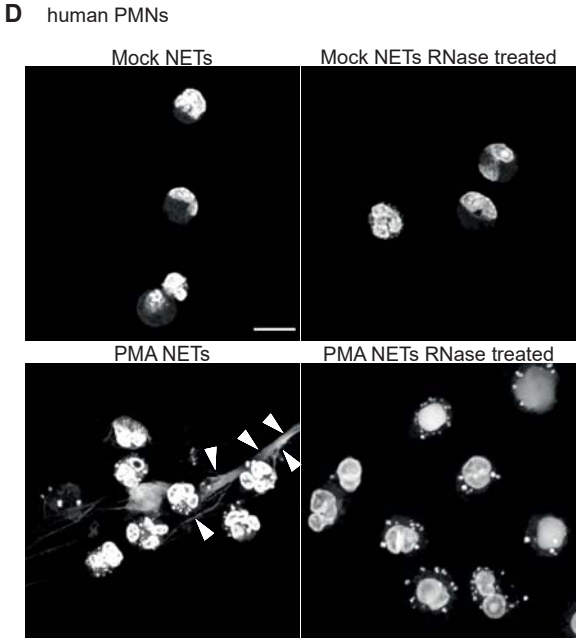
D
human PMNs
Mock NETs
Mock NETs RNase treated
PMA NETs
PMA NETs RNase treated

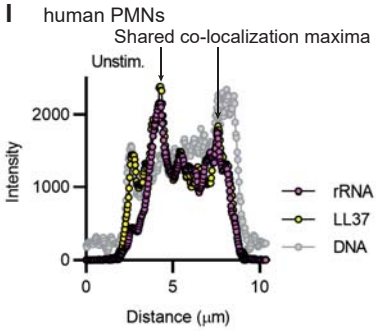
I
human PMNs
Shared co-localization maxima
Unstim.
Intensity
2000
1000
0
0
5
10
Distance (µm)
rRNA
LL37
DNA

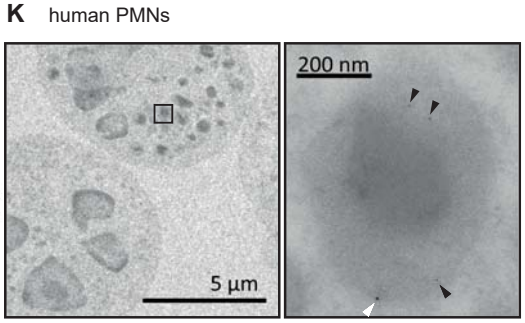
K
human PMNs
200 nm
5 µm

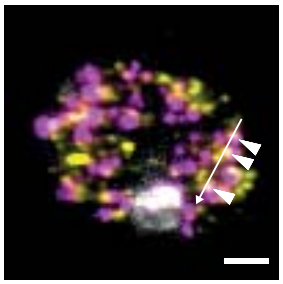
J
human PMNs

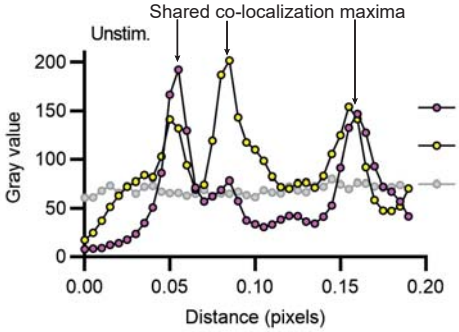
Shared co-localization maxima
Unstim.
Gray value
200
150
100
50
0
0.00
0.05
0.10
0.15
0.20
Distance (pixels)
rRNA
LL37
DNA

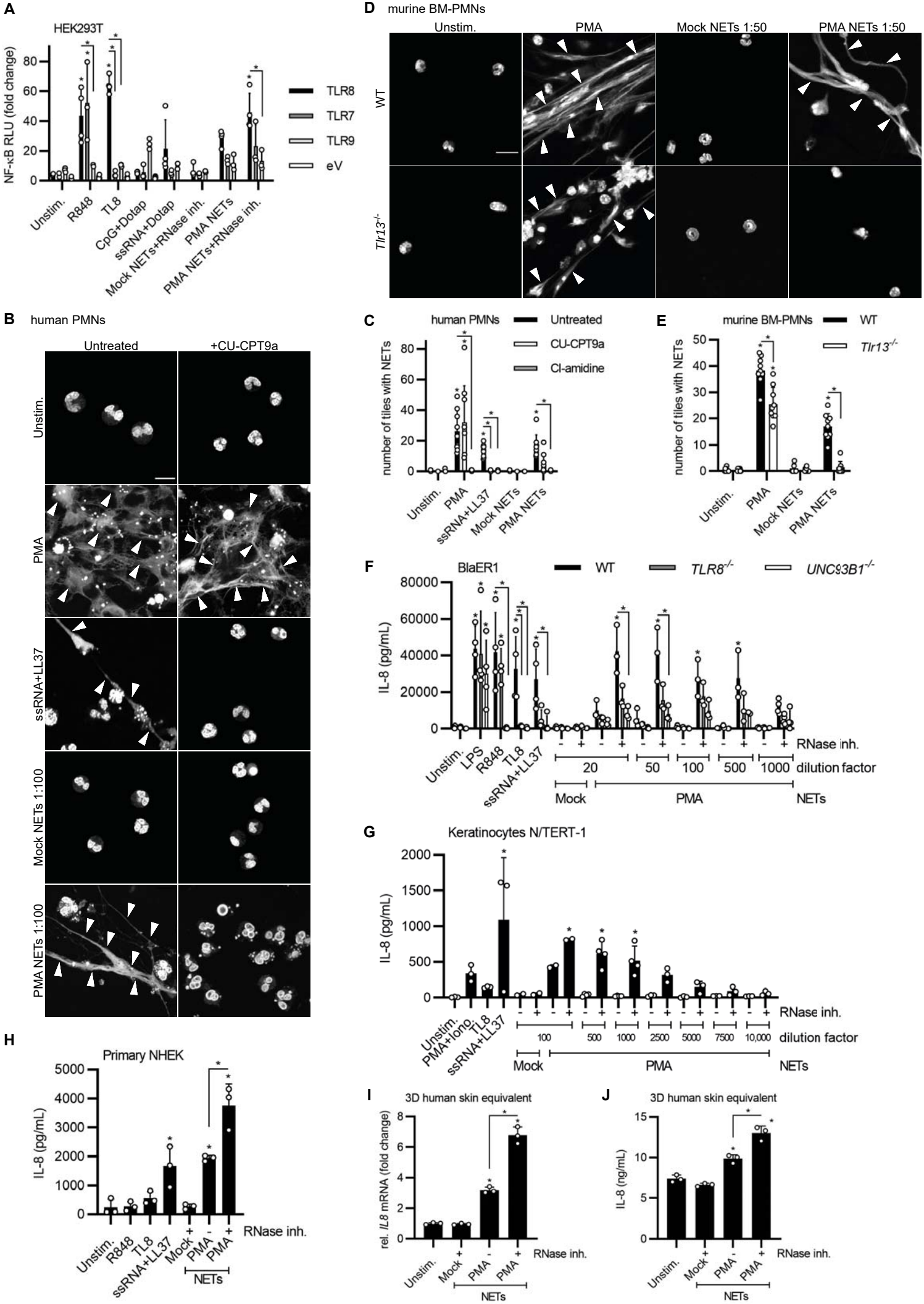
A
HEK293T
NF-κB RLU (fold change)
TLR8
TLR7
TLR9
eV
Unstim.
R848
TL8
CpG+Dotap
ssRNA+Dotap
Mock NETs+RNase inh.
PMA NETs
PMA NETs+RNase inh.
B
human PMNs
Untreated
+CU-CPT9a
Unstim.
PMA
ssRNA+LL37
Mock NETs 1:100
PMA NETs 1:100
C
human PMNs
Untreated
CU-CPT9a
Cl-amidine
number of tiles with NETs
Unstim.
PMA
ssRNA+LL37
Mock NETs
PMA NETs
D
murine BM-PMNs
Unstim.
PMA
Mock NETs 1:50
PMA NETs 1:50
WT
Tlr13-/-
E
murine BM-PMNs
WT
Tlr13-/-
number of tiles with NETs
Unstim.
PMA
Mock NETs
PMA NETs
F
BlaER1
WT
TLR8-/-
UNC93B1-/-
IL-8 (pg/mL)
RNase inh.
Unstim.
LPS
R848
TL8
ssRNA+LL37
20
50
100
500
1000
dilution factor
Mock
PMA
NETs
G
Keratinocytes N/TERT-1
IL-8 (pg/mL)
RNase inh.
Unstim.
PMA+Iono.
TL8
ssRNA+LL37
100
500
1000
2500
5000
7500
10,000
dilution factor
Mock
PMA
NETs
H
Primary NHEK
IL-8 (pg/mL)
RNase inh.
Unstim.
R848
TL8
ssRNA+LL37
Mock
PMA
PMA
NETs
I
3D human skin equivalent
rel. IL8 mRNA (fold change)
RNase inh.
Unstim.
Mock
PMA
PMA
NETs
J
3D human skin equivalent
IL-8 (ng/mL)
RNase inh.
Unstim.
Mock
PMA
PMA
NETs

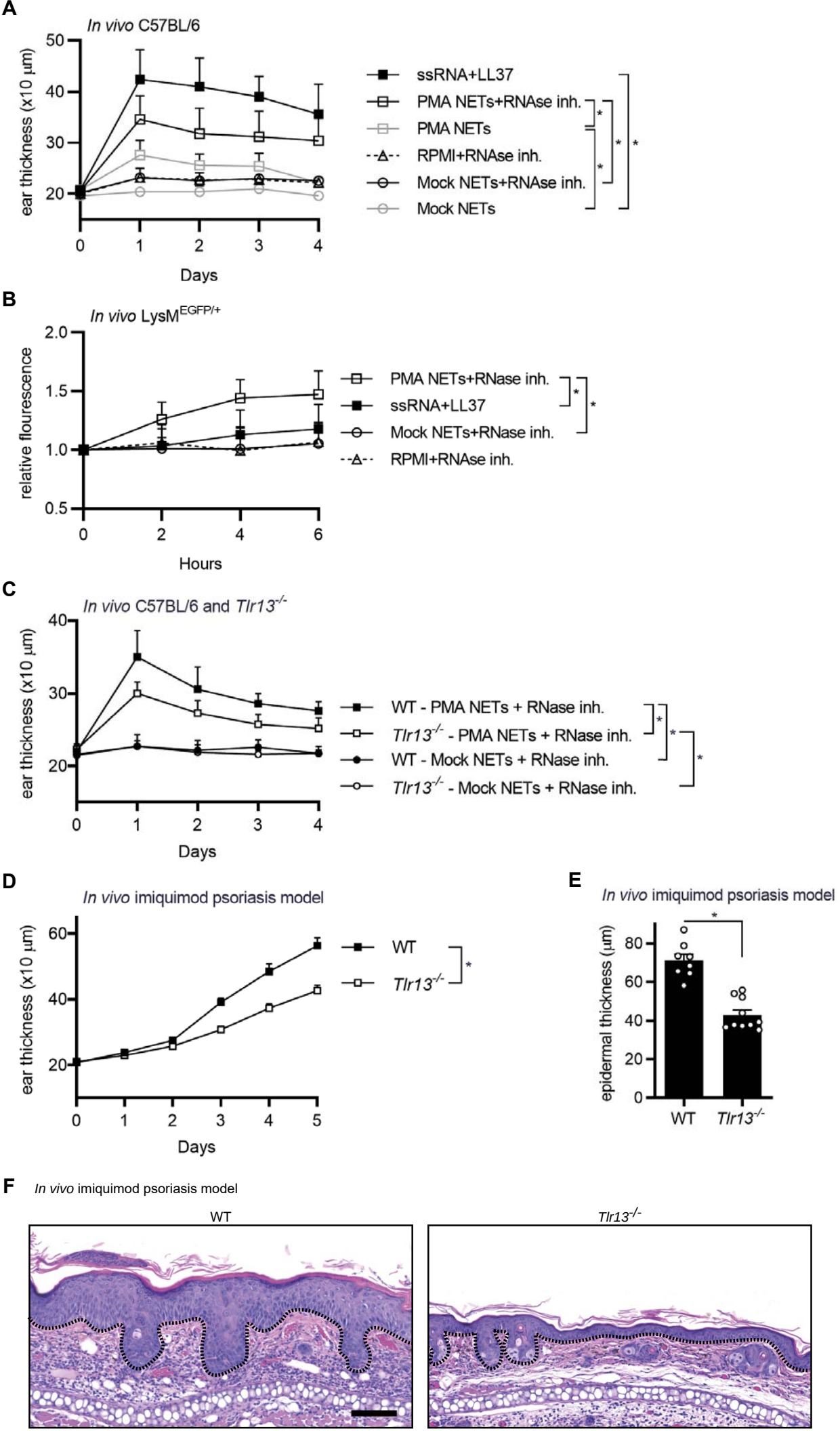
A
In vivo C57BL/6
ear thickness (x10 µm)
Days
ssRNA+LL37
PMA NETs+RNAse inh.
PMA NETs
RPMI+RNAse inh.
Mock NETs+RNAse inh.
Mock NETs
B
In vivo LysM EGFP/+
relative flourescence
Hours
PMA NETs+RNase inh.
ssRNA+LL37
Mock NETs+RNase inh.
RPMI+RNAse inh.
C
In vivo C57BL/6 and Tlr13-/-
ear thickness (x10 µm)
Days
WT - PMA NETs + RNase inh.
Tlr13-/- - PMA NETs + RNase inh.
WT - Mock NETs + RNase inh.
Tlr13-/- - Mock NETs + RNase inh.
D
In vivo imiquimod psoriasis model
ear thickness (x10 µm)
Days
WT
Tlr13-/-
E
In vivo imiquimod psoriasis model
epidermal thickness (µm)
WT
Tlr13-/-
F
In vivo imiquimod psoriasis model
WT
Tlr13-/-